compuscript

Acta Materia Medica

Review Article

Structurally diverse polydopamine-based nanomedicines for cancer therapy

Yuhan Zheng[a,†], Tao Cao[a,†], Xuan Han[b,*], Peng Cao[a,c,d,*] and Qichen Zhan[a,*]

[a]School of Pharmacy, Nanjing University of Chinese Medicine, Nanjing, Jiangsu 210023, China
[b]School of Chinese Medicine, Nanjing University of Chinese Medicine, Nanjing, Jiangsu 210023, China
[c]Affiliated Hospital of Integrated Traditional Chinese and Western Medicine, Nanjing University of Chinese Medicine, Nanjing, Jiangsu 210028, P. R. China
[d]Zhenjiang Hospital of Chinese Traditional and Western Medicine, Zhenjiang, Jiangsu 212002, P. R. China

[†]Y. Zheng and T. Cao contributed equally to this work.
***Correspondence:** hanxuan@njucm.edu.cn (X. Han); cao_peng@njucm.edu.cn (P. Cao); zhanqichen@njucm.edu.cn (Q. Zhan)

Received: 8 July 2022; Revised: 17 September 2022; Accepted: 29 September 2022

Published online: 18 October 2022

DOI 10.15212/AMM-2022-0023

ABSTRACT

Mussel-inspired polydopamine (PDA) has attracted substantial interest in materials synthesis, energy storage, environmental governance, and biomedical science since it was first reported in 2007. PDA, owing to its excellent biocompatibility and photothermal conversion efficiency (η), has been used in photothermal therapy alone and in combination with photodynamic therapy, chemotherapy, radiation therapy, immunotherapy, and gas therapy for cancer treatment. This review summarizes the methods for synthesizing structurally diverse PDA-based nanomedicines and their applications in cancer therapy, to provide perspectives to guide future studies in cancer treatment.

Keywords: polydopamine, nanomedicine, photothermal therapy, synergistic therapies, cancer treatment

1. INTRODUCTION

Despite breakthroughs in medical techniques and increased understanding of cancer, malignant tumors remain the most lethal of diseases [1, 2]. Traditional therapies for cancer have major limitations including severe adverse effects and poor selectivity [3-5]. Recently, with the rapid development of biological nanotechnology, drug delivery systems based on nanomaterials (i.e., nanomedicines) have been widely used in cancer treatment because of their high efficiency, multifunctionality, and low adverse effects [6, 7]. Substantial efforts in the past few years have focused on nanomedicine design to combat cancer [8]. Nanomedicines including liposomes, micelles, polymers, carbon, and inorganic nanoparticles as single or multiple drug carriers can accumulate in tumor tissues through passive targeting (enhanced permeability and retention) and active targeting with labeled targets, thus providing various theranostic and treatment nanoplatforms [9-11].

Mussel-inspired polydopamine (PDA) was first reported by Lee et al. in 2007 [12]. Since then, PDA has been used in biomedical science because of its numerous advantages, such as excellent biocompatibility, low toxicity, and ease of structural modification [13, 14] PDA polymerization shares many common characteristics with eumelanin synthesis [15, 16], and its photothermal conversion efficiency (η) reaches 40% under light irradiation in the near-infrared region [17]. PDA has been applied as a hyperthermia agent in photothermal therapy (PTT) for cancer [18]. Cancer cells are irreversibly damaged when the temperature at tumor tissues exceeds 42 °C, which can easily be achieved by PDA. PTT induces cell apoptosis via cleaving Bid into tBid, regulating mitochondrial membrane potential, and activating the caspase-3 pathway [19, 20]. Notably, PDA has better biocompatibility than nanogold and carbon materials [21, 22]. Owing to its unique physical and chemical properties, PDA structure can be controlled through template or template-free guidance technology. To date, researchers have successfully prepared nanostructured coatings [23], PDA nanospheres [24], nanobowls [25], nanoshells [26], nanocapsules [27], and nanosheets [28], among other structures. The diverse structures of PDA provide many options for building drug delivery systems.

Monotherapy has several limits such as tumor heterogeneity and drug resistance, whereas synergistic

©2022 The Authors. Creative Commons Attribution 4.0 International License

therapies are recognized to be more effective measures for cancer treatment [29-31]. In recent years, many researchers have reviewed the applications of PDA in cancer treatment, but few reviews have focused on the structural control of PDA and its advantages in synergistic anticancer therapy. Herein, we summarize mechanisms of PDA formation and morphological regulation, and PDA's applications in synergistic therapies (PTT/chemotherapy, PPT/CT; PTT/photodynamic therapy, PTT/PDT; PTT/radiation therapy, PTT/RT; PTT/immunotherapy, PTT/IMT; and PTT/gas therapy, PTT/GT). This review aims to provide perspectives regarding the design of PDA-based nanomedicines for cancer treatment (**Figure 1**).

2. POLYMERIZATION MECHANISM

The polymerization mechanism of PDA is complex, and involves extensive covalent bonding, hydrogen-bonding, and π-π stacking interactions [37-39]. Multiple interaction forces endow PDA with excellent stability. PDA can dissolve under only strongly alkaline conditions, thus enabling PDA to be used as a recyclable hyperthermia agent in cancer treatment.

The DA oxidative polymerization mechanism is believed to based on the principle of balanced movement. DA monomers are oxidized to DA quinone and subsequently undergo intramolecular cyclization via 1,4 Michael addition. Subsequently, the molecular rearrangement 5,6-dihydroxylindole (DHI) reacts with oxidative 5,6-indolequinone and forms dimers and other oligomers through a disproportionated reaction [40]. PDA composite layers are generated by crosslinking reactions between these oligomers [41, 42]. However, another commonly believed hypothesis suggests that noncovalent interactions, including charge transfer, π-π stacking, and hydrogen-bond interactions, contribute to the PDA polymerization in addition to covalent bonding. In fact, PDA polymerization shares many characteristics with the pathway of eumelanin synthesis [43]. Similarly to the eumelanin synthesis model, PDA polymerization in water can be divided into three pathways. First, DA monomers tend to form trimers, and then transform into DHI via a cyclization addition reaction. Second, on this basis, these DHI structures allowing for further polymerization are oxidized and fractured to pyrrolic acid. Finally, DA quinone reacts with DHI and generates other oligomers (**Figure 2**).

Despite divergent views regarding the mechanism of PDA polymerization, studies have shown that DA monomers are oxidized to DA-quinone in the initial stage of the reaction [44]. PDA modification accompanied by membrane-like structures indicates that covalent bonds play an essential role in PDA formation [45]. Therefore, a satisfactory theoretical explanation for PDA polymerization is that covalent and noncovalent interactions both contribute to this process.

3. SYNTHESIS METHODS AND STRUCTURE CONTROL

3.1 Template-free method

Lee et al. first reported a method for PDA preparation in alkaline aqueous solutions. PDA, with abundant catechol and amine groups, has excellent adhesive

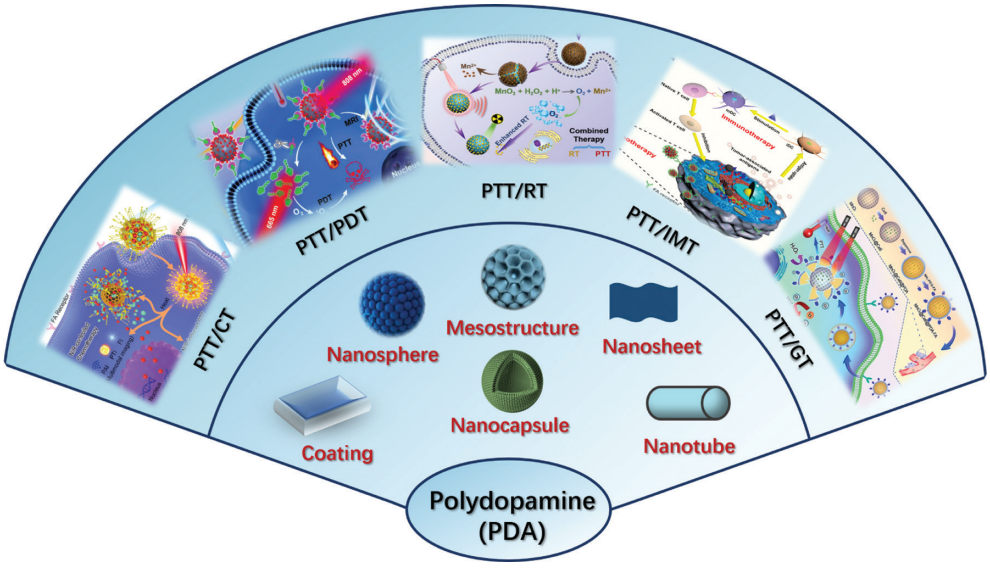

Figure 1 | Structurally diverse PDA, and schematic diagram of PDA-mediated synergistic therapies for cancer therapy (PTT/CT, reproduced with permission [32], copyright 2021 Royal Society of Chemistry; PTT/PDT, reproduced with permission [33], copyright 2019 Wiley-VCH; PTT/RT, reproduced with permission [34], copyright 2019 Elsevier; PTT/IMT, reproduced with permission [35], copyright 2019 American Chemical Society; PTT/GT, reproduced with permission [36], copyright 2020 Elsevier).

©2022 The Authors. Creative Commons Attribution 4.0 International License

Acta Materia Medica

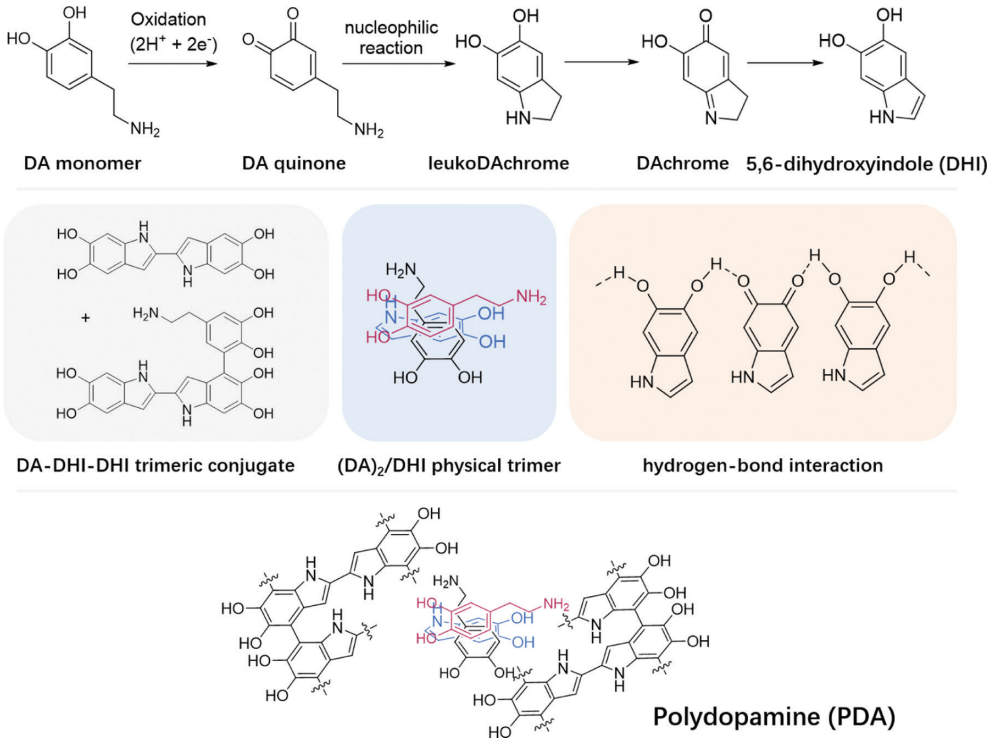

Figure 2 | The polymerization mechanism of PDA.

properties and can deposit on many types of material surfaces [12]. A photograph showing adhesion and the mechanism through which mussels attach to commercial polytetrafluoroethylene are shown in **Figure 3a**. PDA can deposit on nitrocellulose film, coins, and three-dimensional plastic objects (**Figure 3b**). The thickness of the PDA film increases with polymerization time (**Figure 3c**). Similarly to deposition, PDA can also be used to coat the surfaces of nanomaterials including nanogold, nanoFe_3O_4, and nanoSiO_2, thus forming core/shell NPs. These PDA-coated nanoparticles (NPs) can be modified by secondary reactants when they are placed in a solution containing sulfhydryl and amino groups.

Beyond chemical adhesion, mussel-inspired PDA enhances the fibroblast cell adhesion of materials. Hsiao et al. have demonstrated that the adhesion of PDA to cells depends on the pH of the solution. Positively charged materials facilitate bonding with fibronectin and laminin on the cell surfaces. The amino groups on the surface of PDA are protonated and are positively charged under acidic conditions. In contrast, the adhesion of PDA decreases with the deprotonation of amino groups under neutral and alkaline conditions [46, 47]. More importantly, PDA degrades in solid tumors, because the over-expression of lactic acid and hydrogen peroxide break the hydrogen bonds and π-π stacking interactions in PDA [13].

Despite research advances, the slow polymerization rate and unsatisfactory flatness of PDA remain major limitations regarding its application. The introduction of a suitable light source can promote the polymerization of PDA. In 2014, Du et al. reported that PDA polymerization is triggered by UV irradiation at 260 nm [48]. PDA is similar to eumelanin, and UV-treated samples are generally darker than control samples after comparable polymerization times. In contrast, when the UV light source is removed, the polymerization rate of dopamine significantly decreases (**Figure 4a–4c**). This interesting phenomenon has been attributed to the generation of reactive oxygen species (ROS). Moreover, UV irradiation not only accelerates the deposition rate of PDA coating on materials but also significantly increases the secondary modification efficiency [49]. In addition to UV light, microwave irradiation can also accelerate the deposition rate of PDA, as first demonstrated by Lee's group in 2016 [50]. In that study, DA HCl monomers were dissolved in Tris solution (pH 8.5), and then the substrates were immersed in the solution. After microwave irradiation (1000 W, 15 min), the thickness of the PDA coating increased to ~18 nm, whereas the coating thickness reached ~1 nm through a conventional coating (CC) method (**Figure 4d–4f**). Zhang et al. have used $CuSO_4/H_2O_2$ as a trigger to achieve rapid deposition of PDA and have shown that the PDA polymerization rate can be adjusted easily by changing the ratio of $CuSO_4/H_2O_2$ [51]. The rapid homogeneous nucleation of PDA nanoparticles is a key factor in the high uniformity of PDA coating (**Figure 4g–4i**).

©2022 The Authors. Creative Commons Attribution 4.0 International License

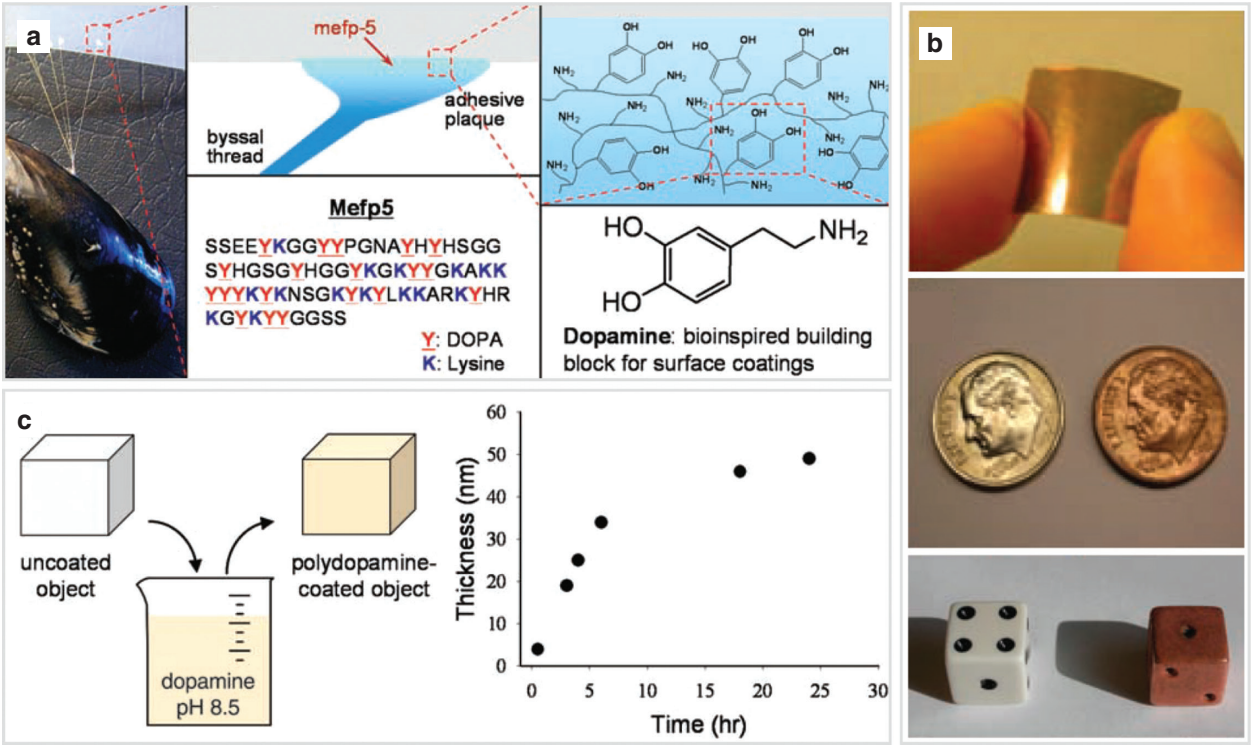

Figure 3 | (a) Photograph showing adhesion and the molecular mechanism of a mussel attaching to commercial polytetrafluoroethylene. (b) PDA-coated nitrocellulose film, coin, and three-dimensional plastic object. (c) Schematic diagram of PDA deposition and the curve of the changing thickness of PDA deposition. Reproduced with permission [12], copyright 2007 Science.

3.2 Template-mediated method

Design and control of nanomaterials with various morphology to meet the requirements of drug delivery systems and tumor microenvironments are major challenges. Owing to its strong adhesion, structurally diverse PDA has been fabricated by using solid templates (inorganic and polymer colloids) or soft templates (vesicles, emulsions, and droplets) via covalent and noncovalent interactions.

Hollow-structure nanomaterials with high drug loading efficiency can decrease drugs' adverse effects and inhibit their enzymatic degradation in drug delivery. As shown in **Figure 5a**, Meng et al. have reported a method for preparing hollow PDA by using a monodisperse silica nanoparticle (SiO_2 NP) template [52]. DA monomers polymerized on the outer surfaces of SiO_2 NPs and formed core/shell SiO_2@PDA NPs under alkaline conditions. The core SiO_2 NPs template was then selectively etched by an HF solution to obtain hollow PDA. In PDA formation, the non-rigid oligomer structure results in molecular folding, which is crucial for supporting template-mediated PDA fabrication. Cui et al. have developed novel dimethyldiethoxysilane emulsion droplets with sizes ranging from hundreds of nanometers to several micrometers for PDA capsule fabrication [27]. These dimethyldiethoxysilane emulsion droplets can be easily removed with ethanol. On the basis of TEM images, all PDA capsules were intact and exhibited fold characteristics (**Figure 5b**). The shell thickness of PDA capsules (10–140 nm) can be controlled easily by adjusting the concentration of DA monomers and the number of polymerization cycles. Xue et al. have synthesized PDA nanotubes by using a solid template comprising nanosized and virgulate curcumin crystals [53]. In brief, DA monomers and curcumin were dispersed in a solution of ethanol/acetone, and a proper quantity of water was added. PDA aggregated on the surfaces of the water-insoluble curcumin crystal template. After the reaction was completed, the curcumin crystal template was removed with ethanol (**Figure 5c**). In general, preparing mesoporous structures through template-mediated PDA fabrication is difficult because of the high cohesive properties and π-π stacking effects. In 2016, Cai et al. reported a method to prepare mesoporous PDA by using triblock copolymer Pluronic F127 and 1,3,5-trimethylbenzene as an organic template, which involved π-π stacking and hydrogen-bonding interactions between PDA and the organic template (**Figure 5d**). The template was removed by extraction with an ethanol and acetone (2:1 v/v) mixture, and the obtained mesoporous PDA was globular with nanosized hollow cavities [54]. Wu et al. first reported a novel method for preparing

©2022 The Authors. Creative Commons Attribution 4.0 International License

Acta Materia Medica

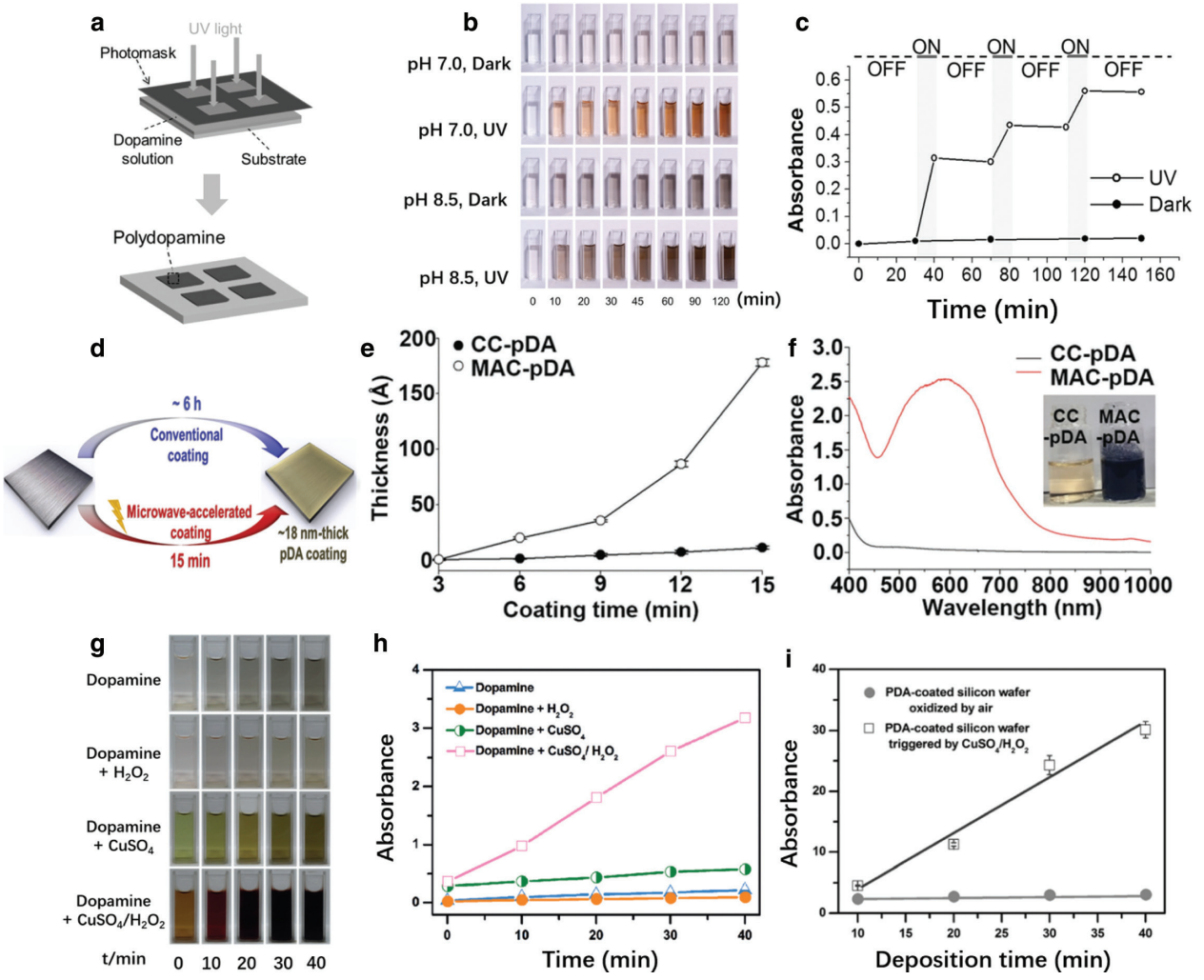

Figure 4 | (a) Schematic diagram of PDA deposition triggered by UV light. (b) Photographs of PDA solutions over time. (c) Changes in the absorbance of PDA solutions under different polymerization conditions (UV irradiation at 254 nm and in the dark). Reproduced with permission [48], copyright 2014 Wiley-VCH. (d) Schematic diagram of PDA deposition triggered by microwaves. (e) Thickness of CC-pDA and MAC-pDA at different coating times. (f) Absorbance of CC-pDA and MAC-pDA. Reproduced with permission [50], copyright 2017 Wiley-VCH. (g) Photographs of PDA formation with different additives. (h) Absorbance intensity curve of PDA at 420 nm. (i) Thickness change in PDA deposited on silicon wafers. Reproduced with permission [51], copyright 2016 Wiley-VCH.

PDA nanoparticles with polypeptide micelles as a template in 2016. PDA polymerization was investigated in a disulfide-bond cross-linked polypeptide micelle group and a control group treated with un-cross-linked dynamic polypeptide micelles. The core-cross-linked polypeptide micelles solution (i.e., PPC micelles) triggered PDA nanoparticle (PPC@PDA) formation, and the average diameters could be controlled by the concentration of PDA and the reaction time. PDA nanoparticles based on the polypeptide micelle template, compared with core-hard templates, showed better safety and biological compatibility *in vivo* (Figure 5e). PDA polymerization guided by soft and hard templates all use the same technique for template removal. Interestingly, Wei et al. have reported a mild, environmentally friendly and nanosized gas template (mainly O_2 and N_2) made by mixing water and water-soluble organic solvents [25]. PDA nanobowls have been prepared on the basis of the template, because the polymerization speed of DA monomers at the solution/air interface is faster than that in solution (Figure 5f). This template-mediated method provides a new reference for fabrication of structurally diverse PDA.

In recent years, with the emergence of two-dimensional (2D) nanomaterials such as graphene, increasing attention has been paid to the possibility of 2D PDA synthesis. Cai et al. reported a DNA-inspired template to construct 2D PDA under a weak alkaline

©2022 The Authors. Creative Commons Attribution 4.0 International License

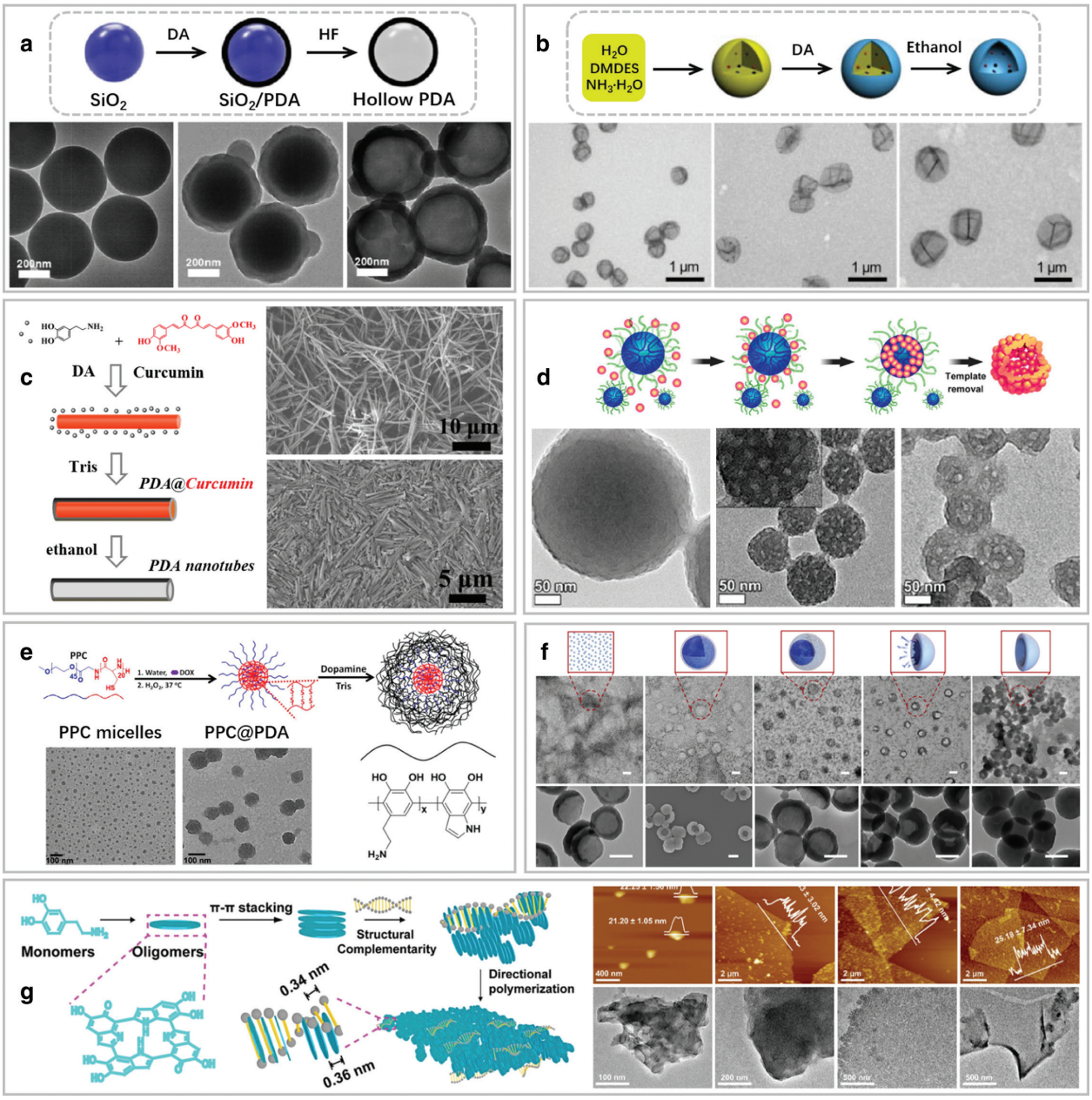

Figure 5 | (a) Schematic diagram of hollow PDA fabrication based on an SiO_2 template, and the corresponding TEM images of SiO_2 nanospheres, SiO_2@PDA, and hollow PDA. Reproduced with permission [52], copyright 2016 American Chemical Society. (b) Schematic diagram of hydrophobic-species-mediated formation of PDA capsules by using emulsion templates. Reproduced with permission [27], copyright 2010 Wiley-VCH. (c) Illustration of the fabrication process of PDA nanotubes based on curcumin crystals. Reproduced with permission [53], copyright 2016 American Chemical Society. (d) Schematic representation of a proposed mechanism for preparation of mesoporous PDA. Reproduced with permission [54], copyright 2016 American Chemical Society. (e) PDA nanoparticle formation based on a polypeptide micelle template. Reproduced with permission [56], copyright 2016 Royal Society of Chemistry. (f) Schematic diagram of PDA nanobowl fabrication based on a gas-bubble template. Reproduced with permission [25], copyright 2021 Elsevier. (g) 2D PDA fabricated on the basis of a DNA template. Reproduced with permission [55], copyright 2019 Royal Society of Chemistry.

solution in 2018. As shown in Figure 5g, the thickness of 2D PDA was comparable to the distance between adjacent nucleotide pairs along the duplex axis of DNA, thus indicating that the specific structural complementarity of DNA contributed to the nanoplatelet formation via lateral packing [55]. In 2019, Zhou et al. proposed an

©2022 The Authors. Creative Commons Attribution 4.0 International License

easily performed method to prepare Janus 2D PDA with an octadecylamine (ODA) template. The ODA formed a reactive bilayer template by self-assembly, and after reaction was covalently linked with DA monomers. Subsequently, PDA oligomers further polymerized on the ODA templates [28]. In summary, PDA with ideal morphology to serve as drug carriers can be chosen to build drug delivery systems according to drug properties and the tumor microenvironment.

In general, template-free methods have been used to prepare PDA nanoparticles and PDA coatings. The nanometric size of PDA nanospheres (or the thickness of PDA coating) can be easily controlled by adjusting the concentration of DA monomers and the reaction time. Moreover, the abundant amino and hydroxyl groups on the PDA surface facilitate secondary modification, thus providing an ideal delivery platform for molecular drugs, such as doxorubicin (DOX), chlorin e6 (Ce6), and paclitaxel (PTX). PDA coatings have been designed as encapsulation films for mesoporous silicon nanomaterials and micro/nano-porous carbon-carrying drugs. The stable PDA coating can protect drugs from enzymatic hydrolysis *in vivo*. In contrast to template-free methods, template-mediated methods can be used to fabricate PDA with desired nanostructures including nanobowls, nanocapsules, mesostructures, nanosheets, and nanotubes. The drug-loading capacity of these PDA structures is higher than that of PDA nanospheres. Furthermore, PDA's unique structures endow it with special functions. For example, Janus PDA is a satisfactory drug carrier to fabricate nanomotors, and PDA nanosheets have multicolor imaging ability in cells, thus providing a variety of opportunities to synthesize nanomedicines for cancer diagnosis and treatment.

4. APPLICATIONS IN CANCER TREATMENT

4.1 PTT monotherapy

DA is the most abundant catecholamine neurotransmitter in the brain. Its polymers (PDA) have excellent biocompatibility and been widely used as drug carriers in cancer treatment. In 2012, Messersmith's group first used PDA-coated Au nanorods as a hyperthermia agent for cancer treatment *in vitro*, and achieved satisfactory treatment results [57]. The strong absorption of PDA in the near-infrared region results in a photothermal conversion rate (η) as high as 40% [58].

In 2013, Lu's group used dopamine melanin colloidal nanospheres (Dpa-melanin CNSs) as a hyperthermia agent to achieve tumor growth suppression in tumor-bearing mice via intravenous injection (**Figure 6a**) [59]. In that study, Dpa-melanin CNSs were prepared through a template-free method in a solution of deionized water and ethanol, and ammonium hydroxide was used to adjust alkalinity. The Dpa-melanin CNSs redispersed well in water and could be stored for serval months without further aggregation. The results of η detection indicated that the temperature of Dpa-melanin CNS aqueous solution (200 μg mL^{-1}) reached 33.6 °C under laser irradiation (2 W cm^{-2}) for 500 s, whereas that of the control increased by only 3.2 °C (**Figure 6b and 6c**). According to the natural cooling temperature change in Dpa-melanin CNSs, the η was calculated to be 40%, thus revealing that Dpa-melanin CNSs are an ideal hyperthermia agent in PTT. The anticancer activity *in vitro* indicated that the inhibitory rate of Dpa-melanin CNSs on cultivated tumor cells (80%) was higher than that in the control group (**Figure 6d and 6e**). After laser irradiation for 5 min, compared with no laser irradiation, the tumor tissues of 4T1-bearing mice showed cell necrosis and ablation, thus further demonstrating the anticancer availability of Dpa-melanin CNSs (**Figure 6f**). The Gd-modified Dpa-melanin CNSs showed excellent magnetic resonance imaging ability *in vivo*. The relaxivity value of Dpa-melanin CNSs was 6.9 mM^{-1} s^{-1}, a value superior to that of commercial Magnevist (**Figure 6g**). This successful attempt *in vivo* has greatly promoted the development of PDA for cancer.

4.2 Synergistic PTT/CT

The heterogeneity, infiltration, and metastasis of tumors are the main obstacles in cancer therapy [60]. Monotherapy to treat malignant tumors has a low cure rate, serious adverse effects, and frequent recurrence [61, 62]. As cancer therapy develops, combination therapies for cancer treatment are being explored. Compared with traditional cancer treatment therapy (operative treatment, CT, and RT), synergistic therapy takes advantages of each therapy, and decreases drug toxicity [63]. Combination therapy based on a nanomaterial platform enables imaging diagnosis for cancer. CT is a common method in clinical cancer treatment, and chemotherapeutic drugs can kill tumors by inhibiting nucleotide metabolism, DNA synthesis, and cell proliferation [64]. However, the CT process causes indiscriminate damage to tumor and normal cells because of the low selectivity of drugs [65]. Decreasing toxic adverse effects and overcoming drug resistance remain substantial challenges. Researchers are increasingly focusing on how to target drug delivery to solid tumor tissues.

James et al. have developed PDA-coated spiky gold nanoparticles (SGNP@PDAs) with excellent photothermal stability (**Figure 7a and 7b**) [66]. In brief, spiky gold nanoparticles (SGNPs) were dispersed in Tris buffer (pH 8.5), and DA HCl was added to the solution and reacted for 30 min. TEM images showed that the thickness of PDA film clearly increased with the concentration of DA monomers (**Figure 7c**). This study revealed that the PDA + laser irradiation combined with DOX clearly increased tumor inhibition efficiency *in vivo*. For evaluation of the anticancer efficiency of drugs, SGNP and SGNP@PDAs were co-incubated with tumor cells. Under laser irradiation (10 W cm^{-2}, 5 min), the cell survival rate of the SGNP@PDA-treated group was lower than that of the SGNP-treated group, thus revealing the high efficiency of photothermal conversion of SGNP@PDAs. The

©2022 The Authors. Creative Commons Attribution 4.0 International License

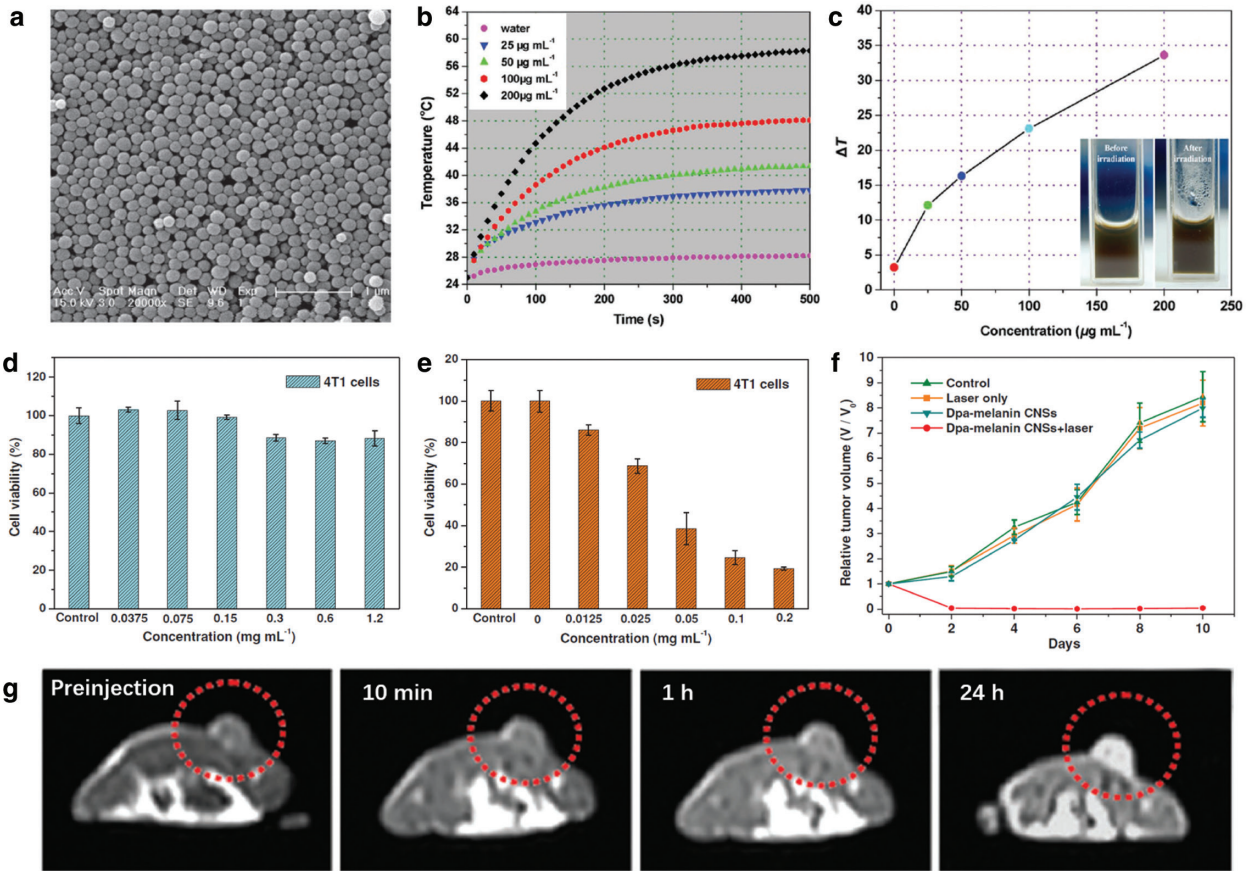

Figure 6 | (a) TEM of Dpa-melanin CNSs. (b) Temperature changes in aqueous Dpa-melanin CNS solutions at different concentrations under laser irradiation, and (c) the corresponding temperature at 500 s. (d) Viability of cells treated with Dpa-melanin CNSs at different concentrations. (e) Viability of cells treated with different concentrations of Dpa-melanin CNSs and laser irradiation (808 nm, 2 W cm^{-2}, 5 min). (f) Relative change in tumor volume in mice treated with different drugs. (g) T_1-weighted MR image of tumor-bearing mice before and after treatment with Gd-DTPA-modified Dpa-melanin CNSs. Reproduced with permission [59], copyright 2013 Wiley-VCH.

results *in vivo* confirmed that the temperature of the SGNP@PDA-treated group increased +13 °C (**Figure 7d**). The SGNP@PDAs efficiently inhibited tumor growth through PTT, and the tumor elimination rate reached 40%. In contrast, after PTT treatment, the tumors of the SGNP-treated group began to re-grow, and all mice were moribund by day 45. More importantly, the combined treatment group (SGNP@PDAs + DOX) showed complete primary-tumor extinction, whereas the tumors treated with SGNP@PDAs alone relapsed by day 20 (**Figure 7e and 7f**). To further investigate the antitumor roles of SGNP@PDAs and DOX, the immune response was assessed in the tumor-bearing mouse model. The distal tumors and relapse suppression were attributed mainly to $CD8^+$ T cells, and NK cells assisted in distal-tumor elimination.

4.3 Synergistic PTT/PDT

Synergistic therapy based on PTT and PDT has been demonstrated to be effective in overcoming tumor heterogeneity. PDT uses a photosensitizer to generate ROS under light irradiation, and tumor cells are damaged by oxidation [67, 68]. However, the main active substance in PDT is singlet oxygen ($^1O_2$), and the lifetime of $^1O_2$ is only approximately 0.04 μs, thus greatly limiting the photosensitizer's extent of damage in cancer treatment [69, 70].

To address this problem, Wei et al. have reported a gas-bubble template for guiding preparation of PDA nanobowls (**Figure 8a**). As shown in **Figure 8b** PDA nanobowls were designed as zinc phthalocyanine (ZnPc) and $Mn(CO)_5Br$ (COMn) carriers to fabricate nanomedicine (PCZNs) [25]. COMn was triggered to release CO in the acidic tumor microenvironment, which could promote the dispersion of PCZN. Therefore, the structure of PDA nanobowls is critical in nanomedicine design, because this asymmetric nanobowl structure accelerates the movement of nanomedicine (**Figure 8c**). The microtopography of PCZNs, as confirmed by TEM and SEM, revealed that PCZNs have a uniformly sized bowl-like structure. For investigating the movement of nanomotors in tumor cells, PDA and PDA + COMn were labeled with a commercial probe (Alexa Fluor 647). Subsequently, the location of PDA and PDA + COMn in live cells was

©2022 The Authors. Creative Commons Attribution 4.0 International License

Acta Materia Medica

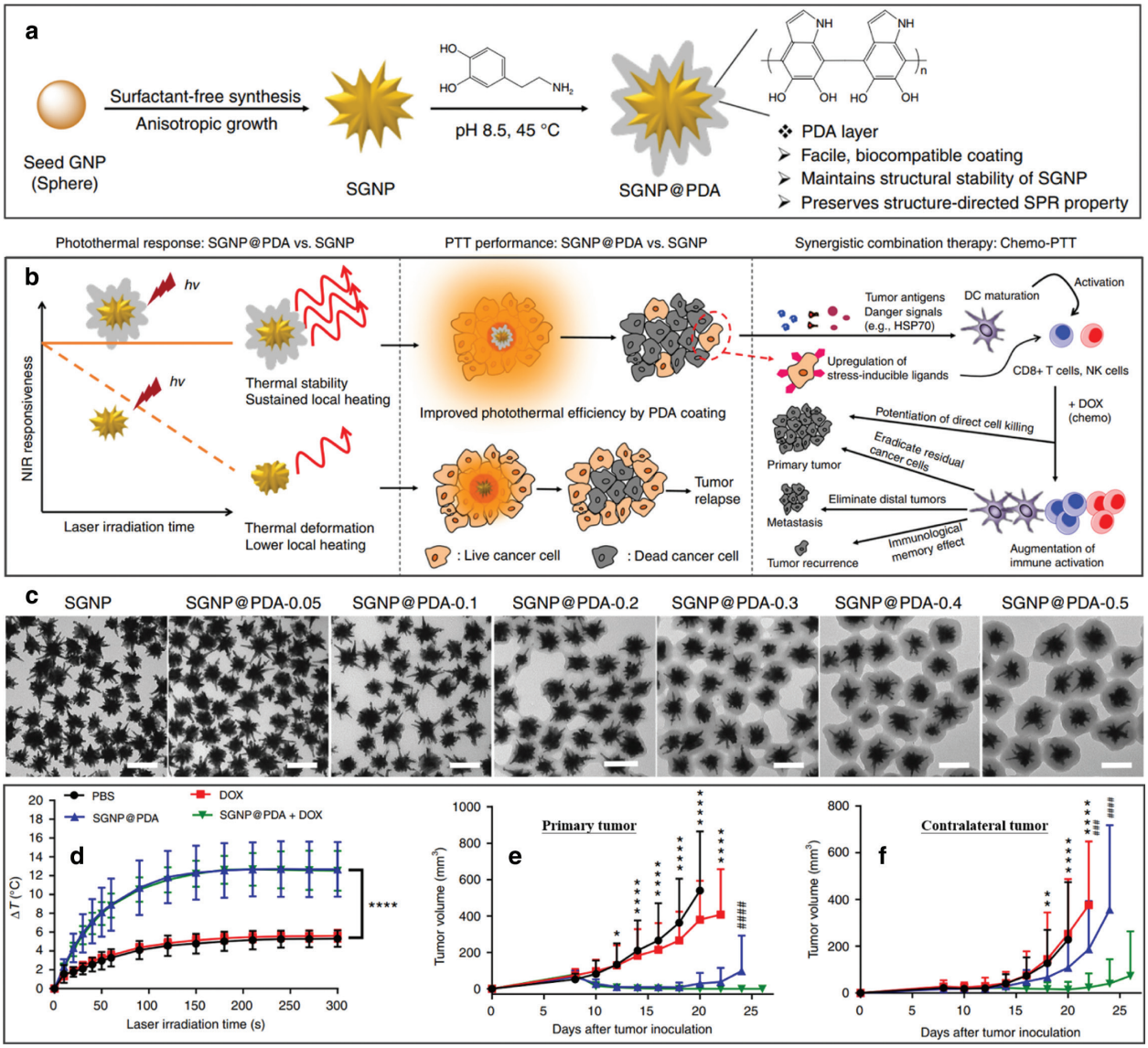

Figure 7 | (a) Schematic diagram of SGNP@PDA fabrication and (b) anticancer mechanism of SGNP@PDA with DOX. (c) TEM images of SGNP@PDA with PDA coating with different concentrations at the same times. (d) Temperature changes in tumors in mice treated with different drugs under laser irradiation. Tumor volume change in tumor-bearing mice in (e) primary tumors and (f) contralateral tumor models. *$P < 0.05$, ***$P < 0.001$, and ****$P < 0.0001$, analyzed by two-way ANOVA (d, e, f), followed by Bonferroni multiple comparisons post-test; * in d, e, f indicates statistically significant differences between SGNP@PDA + DOX vs. PBS or DOX; # in e, f indicates statistically significant differences between SGNP@PDA + DOX vs. SGNP@PDA. Reproduced with permission [66], copyright 2018 Nature.

monitored through c-stochastic optical reconstruction microscopy at different points. In a fixed area and at a fixed z-axis position, c-STORM imaging showed that the position of PDA + COMn changed dramatically while PDA showed slight changes, thus indicating that the movement capability of PDA + COMn was superior to that of PDA. Synergistic tumor cell growth inhibition experiments were performed under normoxic and hypoxic conditions. As shown in Figure 8d and 8e, the anticancer efficiency of PCZNs treated with combination light (808 nm + 665 nm) was higher than that in other groups. Furthermore, tumor growth suppression experiments were performed in tumor-bearing mice. No clear body-weight change was observed in tumor-bearing mice during the treatment, thus indicating that PCZNs have good safety *in vivo* (Figure 8f). After laser irradiation, the tumor volumes of mice treated with different drugs were measured once per day. PDA nanobowls + 808 nm laser irradiation and ZnPc + 665 nm laser irradiation both suppressed tumor growth with PTT and PDT, respectively. The tumor growth suppression efficiency was best with PCZNs and 808 + 665 nm laser irradiation.

©2022 The Authors. Creative Commons Attribution 4.0 International License

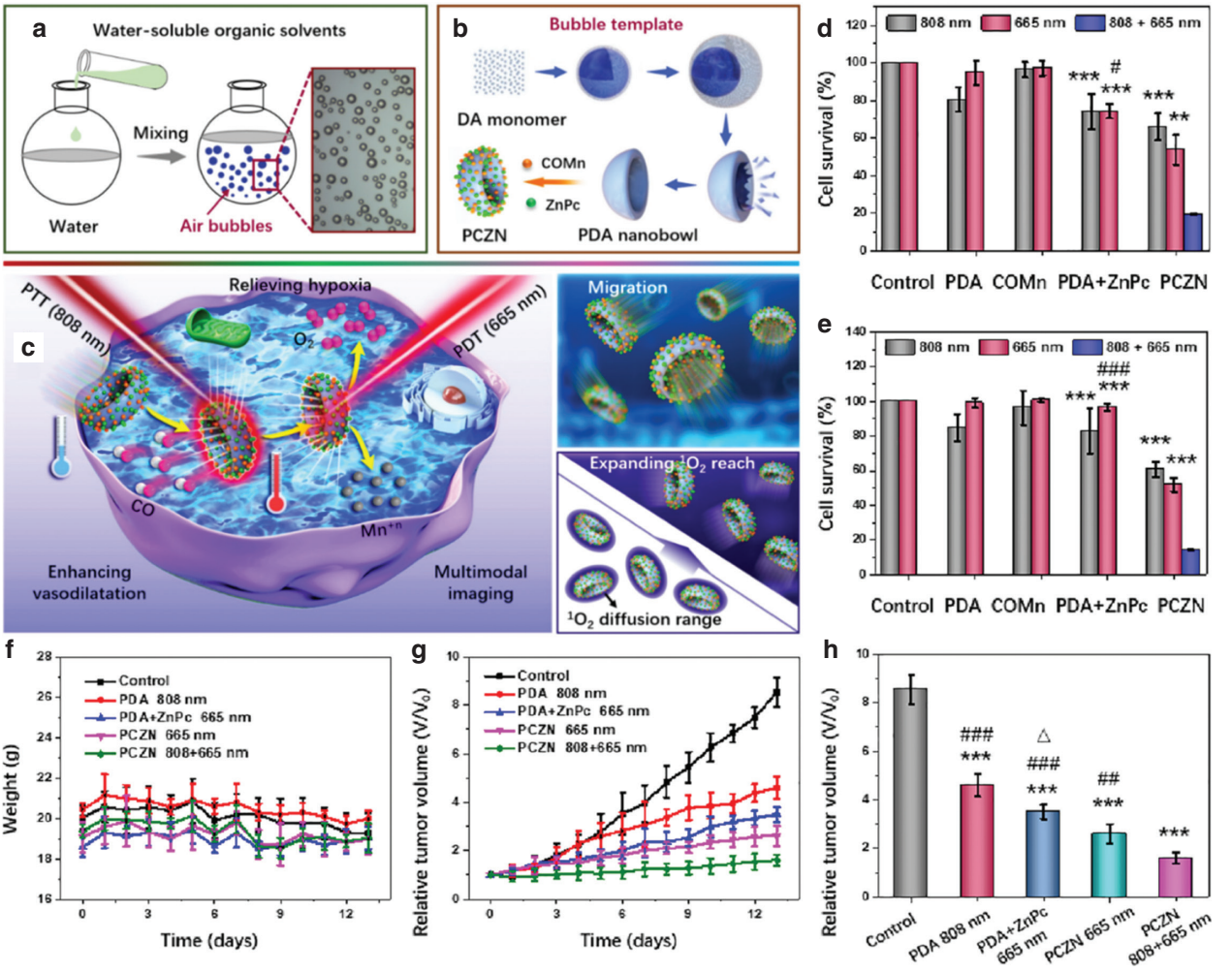

Figure 8 | Schematic diagram of (a) gas-bubble template formation, (b) PCZN fabrication, and (c) its multiple functions. Synergistic tumor cell survival rate after treatment with different drugs under (d) normoxic and (e) hypoxic conditions (P < 0.01, ***P < 0.001 other groups versus PCZNs treated with 808 nm + 665 nm light irradiation group; $^{\#}P$ < 0.05, $^{\#\#\#}P$ < 0.001 PDA + ZnPc treated with 665 nm light irradiation group versus PCZNs treated with 808 nm + 665 nm light irradiation group). (f) Bodyweight change in tumor-bearing mice. (g) Tumor volume changes and (h) comparison of tumor-bearing mice in treatment (***P < 0.001 other groups versus the control; $^{\#\#}P$ < 0.01, $^{\#\#\#}P$ < 0.001 other groups versus PCZNs treated with 808 + 665 nm light irradiation group; $^{\triangle}P$ < 0.05 PDA + ZnPc treated with 665 nm light irradiation group versus PCZNs treated with 665 nm light irradiation group). Reproduced with permission [25], copyright 2021 Elsevier.**

The enhanced PDT activity of PCZNs was ascribed to the movement-derived $^1O_2$ expansion (Figure 8g and 8h). In summary, this research provides a novel synergistic therapy by using nanomotors based on PDA nanobowls to increase the dispersive range of ZnPc in tumor tissue, which may greatly promote the application of PDA in PDT.

Extensive covalent and noncovalent interactions endow PDA with excellent stability. However, in the presence of oxidants or at high temperatures (150 °C), hydroxyl groups in PDA can be oxidized to carbonyl and carboxyl groups, and accompanied by cyclization of amino chains, thus destroying the structure of PDA and promoting its degradation. Consequently, Wei's group has found that 2D PDA or PDA nanosheets can be prepared through a "top-down" exfoliation method using hydrogen peroxide (H_2O_2) as an oxidant (Figure 9a) [45]. Moreover, ultrasound accelerates this exfoliation process. Compared with other morphologies of PDA, 2D PDA shows more efficient drug loading ability because of its high surface area. As shown in Figure 9b, 2D PDA was designed as a carrier for ZnPc to fabricate PZNS nanomedicines. As shown in Figure 9c, the appearance of 2D PDA changed from dark to brown, thus indicating a clear decrease in the polymerization degree of PDA. The morphology of 2D PDA, as observed by TEM and atomic force microscopy, showed a regular lamellar structure and a thickness of 3.4 Å, similar to that of graphene (Figure 9d and 9e). The η of 2D PDA reached 27.6%, and 2D PDA showed good photothermal damage effects both *in vitro* and *in vivo*. As shown in Figure 9f–9h, under combination light irradiation (808 + 665 nm),

©2022 The Authors. Creative Commons Attribution 4.0 International License

Acta Materia Medica

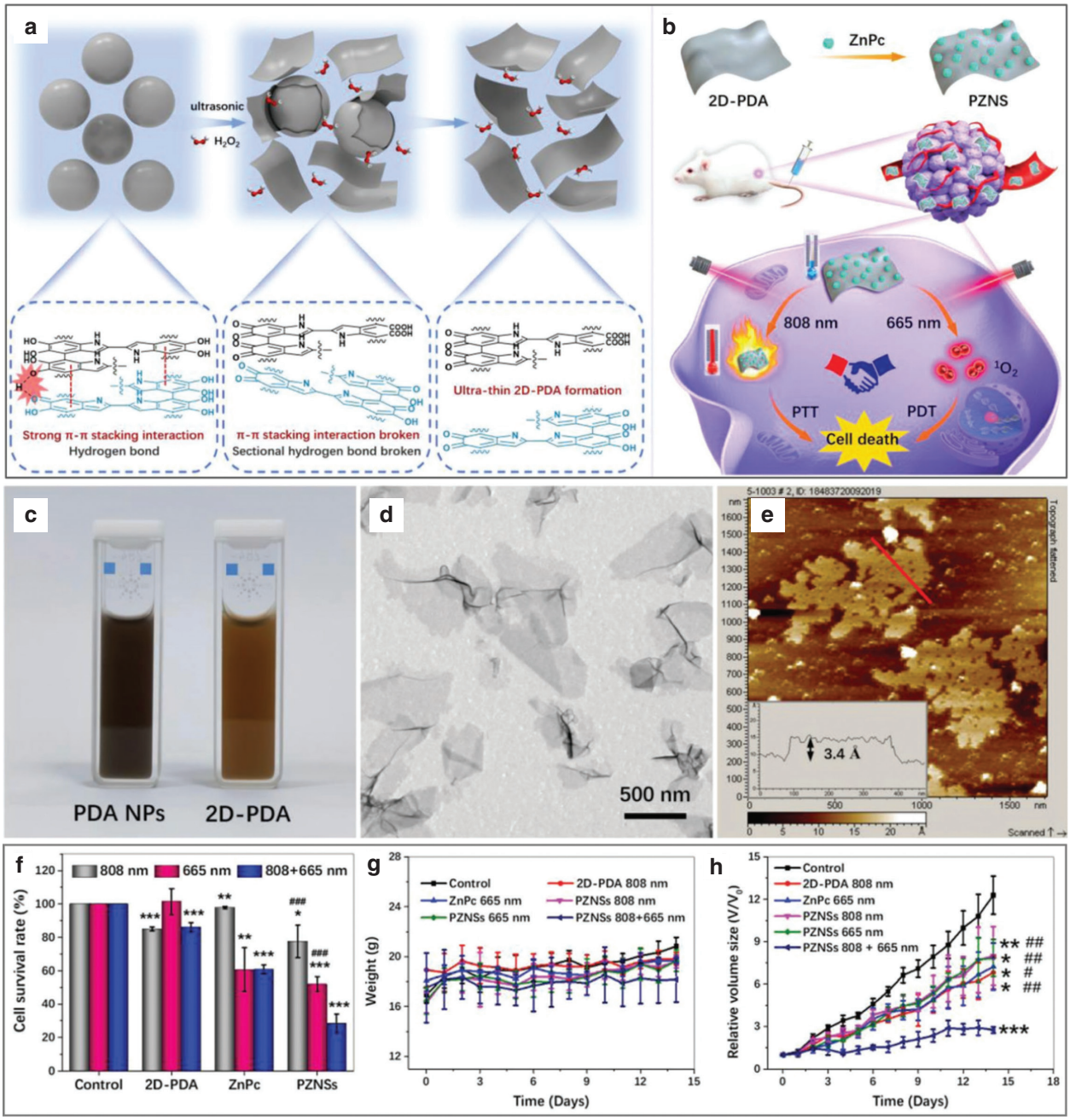

Figure 9 | (a) Schematic diagram of 2D PDA formation by stripping 3D PDA nanospheres. (b) Schematic diagram of nanomedicine preparation based on 2D PDA and ZnPc, and applications in cancer treatment with PTT and PDT. (c) Photographs of PDA NPs and 2D PDA redispersed in distilled water. (d) TEM and (e) atomic force microscopy images of 2D PDA. (f) Anticancer efficiency of different drugs *in vitro* (*$P < 0.001$, **$P < 0.01$, *$P < 0.05$ other groups versus the control; $^{###}P < 0.001$, PZNSs treated with 808 nm light irradiation group, PZNSs treated with 665 nm light irradiation group versus PZNSs treated with 808 nm + 665 nm light irradiation group). (g) Body-weight changes in tumor-bearing mice treated with various drugs. (h) Anticancer efficiency of different drugs *in vivo* (***$P < 0.001$, **$P < 0.01$, *$P < 0.05$ other drugs treated groups versus the control; $^{##}P < 0.01$, $^{#}P < 0.05$ other drugs treated groups versus PZNSs treated with 808 nm + 665 nm light irradiation group). Reproduced with permission [45], copyright 2022 Wiley-VCH.**

the anticancer efficiency of synergistic therapy (PZNSs, PTT + PDT) was higher than that of monotherapy (PTT or PDT).

4.4 Synergistic PTT/RT

RT is a traditional therapy for cancer in clinical settings that uses X-ray (or γ-ray) radiation to kill tumor cells.

©2022 The Authors. Creative Commons Attribution 4.0 International License

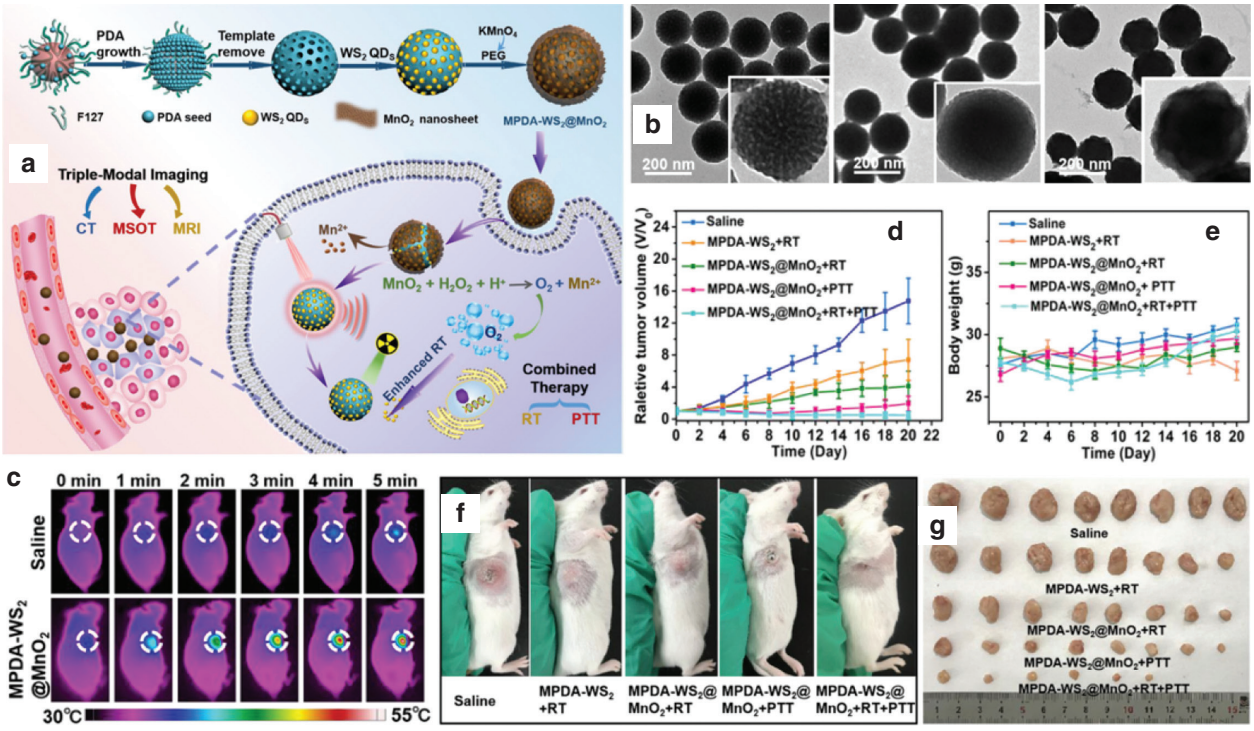

Figure 10 | (a) Schematic diagram of MPDA-WS_2@MnO_2 fabrication and synergistic PTT/RT for cancer treatment. (b) TEM images of MPDA, MPDA-WS_2, and MPDA-WS_2@MnO_2. (c) Photothermal imaging of MPDA-WS_2@MnO_2 in tumor-bearing mice upon laser irradiation at different time points. (d) Relative tumor volume and (e) body weight of mice treated with different drugs for 20 days. (f) Photographs of mice from each group on the 20th day. (g) Photographs of tumors from tumor-bearing mice treated with different drugs. Reproduced with permission [34], copyright 2019 Elsevier.

However, hypoxia, a typical characteristic of solid tumors, severely limits the therapeutic outcomes of RT [71]. The rising temperatures in tumor tissues caused by PTT enhance the blood circulation and increase the O_2 levels in tumors, thus suggesting that synergistic PTT and RT has clear superiority.

Wang et al. have selected mesoporous PDA (MPDA) as vehicle for a radiosensitizer (WS_2 QDs) and manganese dioxide (MnO_2) to fabricate MPDA-WS_2@MnO_2 nanomedicine (**Figure 10a**) [34]. The encapsulation process of WS_2 QDs and MnO_2 was monitored with TME, and the disappearance of mesopores indicated that MPDA had excellent loading capacity for drugs (**Figure 10b**). To study anticancer efficiency *in vivo*, a 4T1 tumor-bearing mouse model was established to detect the photothermal behavior of MPDA-WS_2@MnO_2. As shown in **Figure 10c**, under laser irradiation (1.5 W cm^{-2}, 5 min), the temperature of tumor regions in mice treated with MPDA-WS_2@MnO_2 increased to 54 °C, thus indicating that MPDA-WS_2@MnO_2 facilitates tumor ablation by PTT. Subsequently, the authors investigated the anticancer efficiency of MPDA-WS_2@MnO_2 with PTT and RT *in vivo* (**Figure 10d**) in 4T1 tumor-bearing mice randomly divided into five groups. Compared with the control group, other groups treated with drugs showed tumor growth suppression. Notably, the therapeutic efficiency of mice treated with MPDA-WS_2@MnO_2 + RT was superior to that of MPDA-WS_2 + RT, owing to the O_2 generation ability of MnO_2. The synergistic PTT/RT treatment had significantly better therapeutic effects than the individual therapy. No clear body-weight changes were observed in tumor-bearing mice during the treatment period, thus indicating that these drugs have low toxic effects (**Figure 10e**). After 20 days of treatment, the mice were photographed on the tumor-bearing side, then euthanized to obtain tumors. As shown in **Figure 10f and 10g**, the photograph results were consistent with the outcomes of relative tumor volume. This study has demonstrated that the synergistic PTT/RT based on PDA is a promising method for cancer treatment.

4.5 Synergistic PTT/IMT

IMT is recognized to be a successful therapeutic therapy for cancer, owing to immune-system activation. Although IMT is promising in clinical settings for cancer treatment, a limited number of patients can fully recover with IMT monotherapy because of immune escape. The main aim of IMT is to restore and reverse immune-system deficiencies in the tumor microenvironment. Toll-like receptor agonists and immunomodulatory vaccine adjuvants reprogram the tumor microenvironment [72]. These agonists act either alone or in combination

©2022 The Authors. Creative Commons Attribution 4.0 International License

Acta Materia Medica

with other therapies to generate an anti-tumor immune response. Synergistic PTT/IMT involves PTT-mediated partial ablation of the solid tumor and subsequent release of tumor-associated antigens.

Seth et al. have proposed a strategy using PTT to trigger tumor-associated-antigen release to activate IMT. PDA nanospheres were prepared in water/ethanol mixture by the template-free method and designed as an inner-core thermotherapeutic agent. Subsequently, PDA nanospheres were coated with mesoporous silicon ($mSiO_2$). The immune-stimulating agent (gardiquimod) and 1-tetradecanol were encapsulated in $mSiO_2$ shells [73]. Under NIR laser irradiation, the photothermal properties of PDA adjusted the phase of 1-tetradecanol and controlled gardiquimod release, thus improving cell-based immunotherapy for cancer (Figure 11a). For evaluation of the anticancer behavior of the PDA@$mSiO_2$ *in vivo*, a B16-F10 mouse melanoma model was established, and the mice were divided into four groups randomly. After treatment with drugs for 24 h, the tumor-bearing mice were irradiated with an NIR laser (14 mW mm^{-2}, 5 min). The tumor temperature of PDA@$mSiO_2$ reached 81 °C, whereas that in the PBS-treated group was 40 °C, thereby indicating the high photothermal efficiency and antigen release of PDA@$mSiO_2$. No significant difference was observed in the body weights of tumor-bearing mice, thus indicating

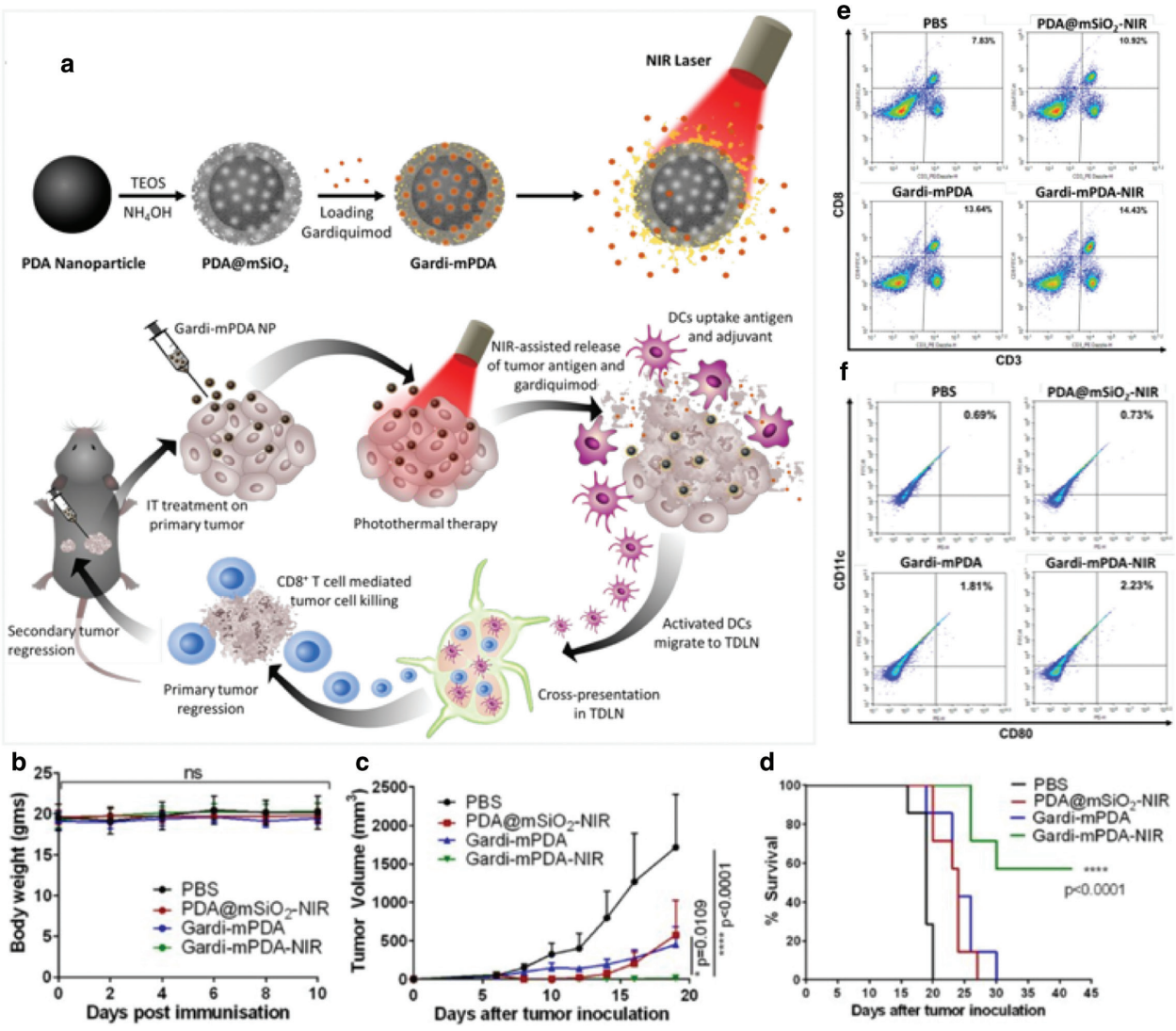

Figure 11 | (a) Schematic illustrations of nanomedicine fabrication and NIR-triggered drug release, and the activation of DCs and effector T cells in cancer treatment. (b) Body weight, (c) tumor volume, and (d) survival curve of tumor-bearing mice during treatment. Immune cells were detected in tumor draining lymph nodes on day 16 (e, $CD3^+$ $CD8^+$ T cells; f, $CD11c^+$ $CD80^+$ dendritic cells). Representative flow cytometry plots of (e) $CD3^+$ and $CD8^+$ T cells and (f) $CD11c^+$ and $CD80^+$ dendritic cells. Reproduced with permission [73], copyright 2020 American Chemical Society.

©2022 The Authors. Creative Commons Attribution 4.0 International License

that PDA@mSiO$_2$ or gardi-mPDA has good safety *in vivo* (Figure 11b). The tumor growth behavior of mice was measured to evaluate the anticancer efficiency of different drugs. As shown in Figure 11c, the tumor growth suppression of gardi-mPDA with NIR laser irradiation was superior to that of gardi-mPDA without NIR laser irradiation and PDA@mSiO$_2$. The mice treated with gardi-mPDA with NIR laser irradiation showed an excellent survival rate (57%) at day 43, whereas the survival in the other groups was 0% at day 30 (Figure 11d). The authors also studied changes in immunological factors, and observed increased T cells and dendritic cells (DCs) in tumor-draining lymph nodes of mice treated with gardi-mPDA + laser irradiation (Figure 11e). Additional maturation markers were measured to assess the maturation of DCs. Compared with PDA@mSiO$_2$ + NIR laser irradiation and the control, the gardi-mPDA-treated group showed higher activation of DCs. Despite emerging evidence of significant immuno-stimulatory effects, the influence of gardi-mPDA is non-specific because of the lack of specific tumor-associated antigen (Figure 11f).

4.6 Synergistic PTT/GT

Gas transmitters, including nitric oxide (NO), carbon monoxide (CO), and hydrogen sulfide (H_2S), are endogenous gas signaling molecules [74]. These transmitters play salient roles in maintaining biological homeostasis and physiological functions. GT for anticancer treatment has received widespread attention in recent years because of its high therapeutic efficacy and biosafety. In fact, the anticancer efficiency of GT is dependent on the concentration and the retention time of gas in solid tumors [75].

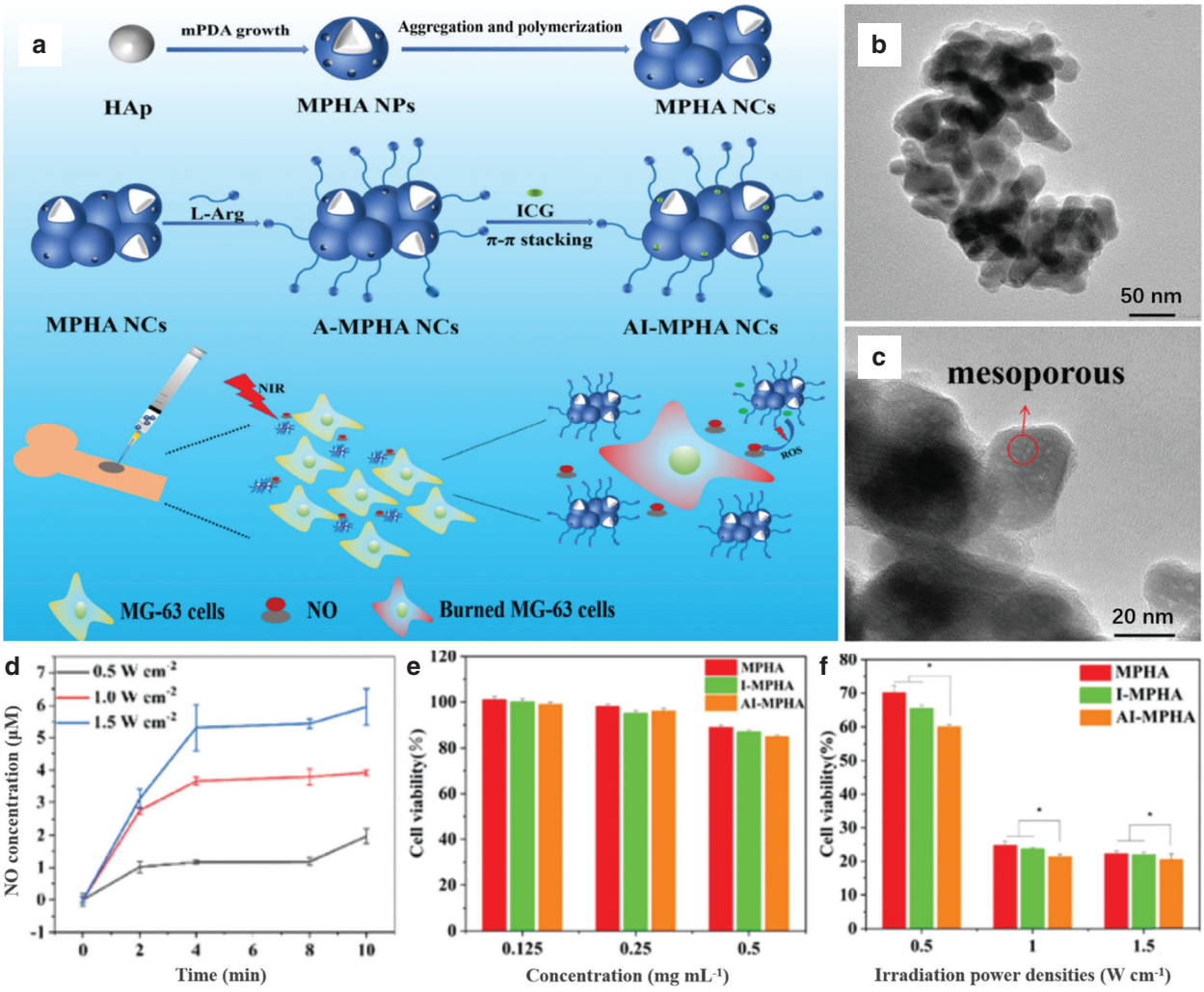

Figure 12 | (a) Schematic diagram of AI-MPHA nanomedicine fabrication, and NO-enhanced PTT with AI-MPHA for anticancer therapy. TEM images of (b) MPHA NCs and (c) MPHA NCs. (d) NO release behaviors from AI-MPHA NCs under near-infrared light irradiation (0.5, 1.0, and 1.5 W cm^{-2}). (e) Dark toxicity and (f) phototoxicity of different drugs in MG-63 cells. Reproduced with permission [76], copyright 2021 Royal Society of Chemistry.

©2022 The Authors. Creative Commons Attribution 4.0 International License

Zhao's group has constructed a drug delivery system based on mesoporous PDA (MPDA) [76]. prepared with Pluronic F127 and TMB as soft templates. As shown in **Figure 12a**, hydroxyapatite (HAp) nanoparticles were coated with PDA, and the templates were removed with a solution of acetone and ethanol to form mesoporous core-shell structure nanocomposites (MPDA@HAp nano-composites, or MPHA NCs). As shown in **Figure 12b and 12c**, TEM indicated that the MPHA NCs had a porous structure. This mesoporous structure endowed MPHA NCs with high L-Arg (NO donor) and indocyanine green (ICG) loading efficiency, and the nanomedicine was denoted AI-MPHA NCs. AI-MPHA NCs generated ROS, inducing the catalysis of L-Arg to release NO under near-infrared light irradiation. With an increase in laser power, the NO release rate clearly increased (**Figure 12d**). The anticancer efficiency of AI-MPHA NCs was assessed in MG-63 human osteosarcoma cells. After incubation with cells, all drugs showed excellent safety without light irradiation (**Figure 12e**). In contrast, after laser irradiation (1.0 W cm^{-2}) for 10 min, the viability of cells treated with AI-MPHA NCs (0.25 mg mL^{-1}) decreased to 23.6%. More importantly, under the same laser irradiation conditions, the repression rate of tumor cell growth in the AI-MPHA NC group was superior to that in the MPHA NC and I-MPHA NC groups, thus suggesting that the NO showed synergetic effects with photothermal treatment in MG-63 cell ablation (**Figure 12f**).

Table 1 | Summary of PDA-based nanomedicine in synergistic therapy for cancer.

PDA type	Drug combination	Tumor cells	Therapy	Ref.
Coating	DOX	HeLa	PTT/CT	[77]
Coating	PTX	HeLa	PTT/CT	[78]
Coating	/	4T1	PTT/RT	[79]
Coating	Ce6	4T1	PTT/PDT	[80]
Coating	SO_2	4T1	PTT/GT	[81]
Nanosphere	BTZ	CT26	PTT/CT	[82]
Nanosphere	Ce6	HepG2	PTT/PDT	[83]
Nanosphere	DOXO	HeLa	PTT/CT	[84]
Core/shell	DOX	HeLa	PTT/CT	[85]
Core/shell	ICG	HeLa	PTT/PDT	[86]
Core/shell	Ce6	4T1	PTT/PDT	[87]
Core/shell	/	MCF-7	PTT/IMT	[88]
Nanocapsule	DOX	MCF-7	PTT/CT	[89]
Hollow structure	Ce6	B16F10	PTT/PDT	[90]
Hollow structure	DOX	4T1	PTT/CT	[91]
Hollow structure	DOX	HeLa	PTT/CT	[92]

In addition to the above examples, we also summarize several nanomedicines based on structurally diverse PDA, and their synergistic therapies for cancer treatment. The PDA types, cancer types, and synergistic therapies are listed in **Table 1**.

5. CONCLUSIONS AND PERSPECTIVES

In conclusion, this review summarized structurally diverse PDA, its synthetic methods, and its applications as a hyperthermia agent for synergistic therapies in cancer treatment. Multiple morphologies of PDA can be prepared via self-polymerization under mild conditions, and PDA nanomaterials are ideal carriers for drugs to construct nanomedicines, owing to their excellent biocompatibility, biodegradation, and high photothermal conversion efficiency.

Nanomaterials generally lack active tumor-targeting ability and tumor selectivity, thus limiting their therapeutic efficiency, and may cause irreversible adverse effects. To overcome these drawbacks, secondary modification of the abundant amino and hydroxyl groups of PDA, such as RGD peptide, folic acid, larotrectinib, and anti-EGFR, is promising for tumor targeting. In addition, dual targeting based on active and passive targeting (enhanced permeability and retention effect) is expected to further improve the enrichment of drugs in solid tumors.

How to integrate diagnosis and treatment platforms has become a major area of current nanomedicine research. Nuclear magnetic resonance technology is widely used for disease diagnosis in clinical settings, and contrast medium is a key component of this technology. PDA has strong complexation ability to metal ions including Gd, Mn, and Fe. To date PDA-based magnetic contrast technology has achieved great success, as demonstrated in tumor-bearing mice.

Although PDA-based nanomedicine has a bright future in cancer therapy, some uncertainties involving PDA synthesis and applications remain. First, how to achieve large-scale synthesis of PDA with uniform size is a major challenge. Second, because of strong adhesion, how to avoid PDA agglomeration in solution must be considered in future studies. Third, the interactions between PDA and biological systems (living cells, hormones, proteins, and immune systems) have largely been overlooked. Finally, research on the long-term stability and toxicity of PDA *in vivo*, and how PDA is biodegraded and eliminated from the body, must be performed. We hope that this review will contribute to the understanding of PDA synthesis and its applications in cancer treatment.

ACKNOWLEDGMENTS

This work was financially supported by the National Natural Science Foundation of China (grant no. 82104686) and Nanjing University of Chinese Medicine (XPT82104686).

©2022 The Authors. Creative Commons Attribution 4.0 International License

CONFLICTS OF INTEREST

The authors declare no conflicts of interest.

REFERENCES

[1] Sung H, Ferlay J, Siegel RL, Laversanne M, Soerjomataram I, Jemal A, et al.: Global Cancer Statistics 2020: Globocan Estimates of Incidence and Mortality Worldwide for 36 Cancers in 185 Countries. *CA: A Cancer Journal for Clinicians* 2021, 71:209–249.

[2] Mou C, Yang Y, Bai Y, Yuan P, Wang Y, Zhang L: Hyaluronic Acid and Polydopamine Functionalized Phase Change Nanoparticles for Ultrasound Imaging-Guided Photothermal-Chemotherapy. *Journal of Materials Chemistry B* 2019, 7:1246–1257.

[3] Housman G, Byler S, Heerboth S, Lapinska K, Longacre M, Snyder N, et al.: Drug Resistance in Cancer: An Overview. *Cancers* 2014, 6:1769–1792.

[4] Wood GE, Hockings H, Hilton DM, Kermorgant S: The Role of Met in Chemotherapy Resistance. *Oncogene* 2021, 40:1927–1941.

[5] Fiorino C, Jeraj R, Clark CH, Garibaldi C, Georg D, Muren L, et al.: Grand Challenges for Medical Physics in Radiation Oncology. *Radiotherapy and Oncology* 2020, 153:7–14.

[6] Hui Y, Yi X, Hou F, Wibowo D, Zhang F, Zhao D, et al.: Role of Nanoparticle Mechanical Properties in Cancer Drug Delivery. *ACS Nano* 2019, 13:7410–7424.

[7] Rawal S, Patel MM: Threatening Cancer with Nanoparticle Aided Combination Oncotherapy. *Journal of Controlled Release* 2019, 301:76–109.

[8] Seeta Rama Raju G, Benton L, Pavitra E, Yu JS: Multifunctional Nanoparticles: Recent Progress in Cancer Therapeutics. *Chemical Communications* 2015, 51:13248–13259.

[9] Gong F, Yang N, Wang X, Zhao Q, Chen Q, Liu Z, et al.: Tumor Microenvironment-Responsive Intelligent Nanoplatforms for Cancer Theranostics. *Nano Today* 2020, 32:100851.

[10] Bort G, Lux F, Dufort S, Crémillieux Y, Verry C, Tillement O: EPR-Mediated Tumor Targeting Using Ultrasmall-Hybrid Nanoparticles: From Animal to Human with Theranostic Aguix Nanoparticles. *Theranostics* 2020, 10:1319–1331.

[11] Goddard ZR, Marin MJ, Russell DA, Searcey M: Active Targeting of Gold Nanoparticles as Cancer Therapeutics. *Chemical Society Reviews* 2020, 49:8774–8789.

[12] Lee H, Dellatore SM, Miller WM, Messersmith PB: Mussel-Inspired Surface Chemistry for Multifunctional Coatings. *Science* 2007, 318:426–430.

[13] Wu Q, Niu M, Chen X, Tan L, Fu C, Ren X, et al.: Biocompatible and Biodegradable Zeolitic Imidazolate Framework/Polydopamine Nanocarriers for Dual Stimulus Triggered Tumor Thermo-Chemotherapy. *Biomaterials* 2018, 162:132–143.

[14] Lin L-S, Cong Z-X, Cao J-B, Ke K-M, Peng Q-L, Gao J, et al.: Multifunctional fe3o4@polydopamine Core–Shell Nanocomposites for Intracellular MRNA Detection and Imaging-Guided Photothermal Therapy. *ACS Nano* 2014, 8:3876–3883.

[15] d'Ischia M, Napolitano A, Ball V, Chen C-T, Buehler MJ: Polydopamine and Eumelanin: From Structure–Property Relationships to a Unified Tailoring Strategy. *Accounts of Chemical Research* 2014, 47:3541–3550.

[16] Chen CT, Martin-Martinez FJ, Jung GS, Buehler MJ: Polydopamine and Eumelanin Molecular Structures Investigated with ab initio Calculations. *Chemical Science* 2017, 8:1631–1641.

[17] Liu Y, Ai K, Lu L: Polydopamine and its Derivative Materials: Synthesis and Promising Applications in Energy, Environmental, and Biomedical Fields. *Chemical Reviews* 2014, 114:5057–5115.

[18] Ding F, Gao X, Huang X, Ge H, Xie M, Qian J, et al.: Polydopamine-Coated Nucleic Acid Nanogel for Sirna-Mediated Low-Temperature Photothermal Therapy. *Biomaterials* 2020, 245:119976.

[19] Melamed JR, Edelstein RS, Day ES: Elucidating the Fundamental Mechanisms of Cell Death Triggered by Photothermal Therapy. *ACS Nano* 2015, 9:6–11.

[20] Pérez-Hernández M, del Pino P, Mitchell SG, Moros M, Stepien G, Pelaz B, et al.: Dissecting the Molecular Mechanism of Apoptosis During Photothermal Therapy Using Gold Nanoprisms. *ACS Nano* 2015, 9:52–61.

[21] Yang J, Dai D, Lou X, Ma L, Wang B, Yang YW: Supramolecular Nanomaterials Based on Hollow Mesoporous Drug Carriers and Macrocycle-Capped CuS Nanogates for Synergistic Chemo-Photothermal Therapy. *Theranostics* 2020, 10:615–629.

[22] Ma H, Li S, Zhang H, Wei Y, Jiang L: Fabrication of Polydopamine-Based Layer-by-Layer Nanocomposites for Combined pH-Sensitive Chemotherapy and Photothermal Therapy. *Colloids and Surfaces A: Physicochemical and Engineering Aspects* 2019, 561:332–340.

[23] Lynge ME, van der Westen R, Postma A, Städler B: Polydopamine-a Nature-Inspired Polymer Coating for Biomedical Science. *Nanoscale* 2011, 3:4916–4928.

[24] Ghorbani F, Zamanian A, Behnamghader A, Joupari MD: A Facile Method to Synthesize Mussel-Inspired Polydopamine Nanospheres as an Active Template for In Situ Formation of Biomimetic Hydroxyapatite. *Materials Science and Engineering: C* 2019, 94:729–739.

[25] Zhan Q, Shi X, Fan D, Zhou L, Wei S: Solvent Mixing Generating Air Bubbles as a Template for Polydopamine Nanobowl Fabrication: Underlying Mechanism, Nanomotor Assembly and Application in Cancer Treatment. *Chemical Engineering Journal* 2021, 404:126443.

[26] Dong Z, Feng L, Hao Y, Chen M, Gao M, Chao Y, et al.: Synthesis of Hollow Biomineralized CaCO3–Polydopamine Nanoparticles for Multimodal Imaging-Guided Cancer Photodynamic Therapy with Reduced Skin Photosensitivity. *Journal of the American Chemical Society* 2018, 140:2165–2178.

[27] Cui J, Wang Y, Postma A, Hao J, Hosta-Rigau L, Caruso F: Monodisperse Polymer Capsules: Tailoring Size, Shell Thickness, and Hydrophobic Cargo Loading via Emulsion Templating. *Advanced Functional Materials* 2010, 20:1625–1631.

[28] Sheng W, Li W, Yu B, Li B, Jordan R, Jia X, et al.: Mussel-Inspired Two-Dimensional Freestanding Alkyl-Polydopamine Janus Nanosheets. *Angewandte Chemie International Edition* 2019, 58:12018–12022.

[29] Liang P, Ballou B, Lv X, Si W, Bruchez MP, Huang W, et al.: Monotherapy and Combination Therapy Using Anti-Angiogenic Nanoagents to Fight Cancer. *Advanced Materials* 2021, 33:2005155.

[30] Tilija Pun N, Jeong C-H: Statin as a Potential Chemotherapeutic Agent: Current Updates as a Monotherapy, Combination Therapy, and Treatment for Anti-Cancer Drug Resistance. *Pharmaceuticals* 2021, 14:470.

©2022 The Authors. Creative Commons Attribution 4.0 International License

[31] Wu C, Wang H, Wei Z, Li C, Luo Z: Polydopamine-Mediated Surface Functionalization of Electrospun Nanofibrous Membranes: Preparation, Characterization and their Adsorption Properties Towards Heavy Metal Ions. *Applied Surface Science* 2015, 346:207–215.

[32] Gao P, Wei R, Liu X, Chen Y, Wu T, Shi M, et al.: Covalent Organic Framework-Engineered Polydopamine Nanoplatform for Multimodal Imaging-Guided Tumor Photothermal-Chemotherapy. *Chemical Communications* 2021, 57:5646–5649.

[33] Zhan Q, Shi X, Zhou J, Zhou L, Wei S: Drug-Controlled Release Based on Complementary Base Pairing Rules for Photodynamic-Photothermal Synergistic Tumor Treatment. *Small* 2019, 15:1803926.

[34] Wang Y, Song S, Lu T, Cheng Y, Song Y, Wang S, et al.: Oxygen-Supplementing Mesoporous Polydopamine Nanosponges with WS_2 QDs-Embedded for CT/MSOT/MR Imaging and Thermoradiotherapy of Hypoxic Cancer. *Biomaterials* 2019, 220:119405.

[35] Chen R, Zhu C, Fan Y, Feng W, Wang J, Shang E, et al.: Polydopamine-Based Multifunctional Platform for Combined Photothermal Therapy, Chemotherapy, and Immunotherapy in Malignant Tumor Treatment. *ACS Applied Bio Materials* 2019, 2:874–883.

[36] Zeng W, Zhang H, Deng Y, Jiang A, Bao X, Guo M, et al.: Dual-Response Oxygen-Generating MnO_2 Nanoparticles with Polydopamine Modification for Combined Photothermal-Photodynamic Therapy. *Chemical Engineering Journal* 2020, 389:124494.

[37] Simon JD, Peles DN: The Red and the Black. *Accounts of Chemical Research* 2010, 43:1452–1460.

[38] Schaubroeck D, Vercammen Y, Van Vaeck L, Vanderleyden E, Dubruel P, Vanfleteren J: Surface Characterization and Stability of an Epoxy Resin Surface Modified with Polyamines Grafted on Polydopamine. *Applied Surface Science* 2014, 303:465–472.

[39] Bernsmann F, Ball V, Addiego F, Ponche A, Michel M, Gracio JJdA, et al.: Dopamine-Melanin Film Deposition Depends on the Used Oxidant and Buffer Solution. *Langmuir* 2011, 27:2819–2825.

[40] Dreyer DR, Miller DJ, Freeman BD, Paul DR, Bielawski CW: Elucidating the Structure of Poly(dopamine). *Langmuir* 2012, 28:6428–6435.

[41] Hong S, Na YS, Choi S, Song IT, Kim WY, Lee H: Non-Covalent Self-Assembly and Covalent Polymerization Co-Contribute to Polydopamine Formation. *Advanced Functional Materials* 2012, 22:4711–4717.

[42] Chen CT, Buehler MJ: Polydopamine and Eumelanin Models in Various Oxidation States. *Physical Chemistry Chemical Physics* 2018, 20:28135–28143.

[43] Alfieri ML, Micillo R, Panzella L, Crescenzi O, Oscurato SL, Maddalena P, et al.: Structural Basis of Polydopamine Film Formation: Probing 5,6-dihydroxyindole-Based Eumelanin Type Units and the Porphyrin Issue. *ACS Applied Materials & Interfaces* 2018, 10:7670–7680.

[44] Della Vecchia NF, Avolio R, Alfè M, Errico ME, Napolitano A, d'Ischia M: Building-Block Diversity in Polydopamine Underpins a Multifunctional Eumelanin-Type Platform Tunable Through a Quinone Control Point. *Advanced Functional Materials* 2013, 23:1331–1340.

[45] Zhan Q, Shi X, Jiang B, Zheng Y, Zhou L, Cao P, et al.: Two-Dimensional Polydopamine Fabrication by a Mild Oxidation-Based Exfoliation Route and its Application for Cancer Treatment. *Advanced Materials Interfaces* 2022, 9:2200440.

[46] Hsiao C-W, Bai M-Y, Chang Y, Chung M-F, Lee T-Y, Wu C-T, et al.: Electrical Coupling of Isolated Cardiomyocyte Clusters Grown on Aligned Conductive Nanofibrous Meshes for their Synchronized Beating. *Biomaterials* 2013, 34:1063–1072.

[47] Leal-Egaña A, Díaz-Cuenca A, Boccaccini AR: Tuning of Cell-Biomaterial Anchorage for Tissue Regeneration. *Advanced Materials* 2013, 25:4049–4057.

[48] Du X, Li L, Li J, Yang C, Frenkel N, Welle A, et al.: Uv-Triggered Dopamine Polymerization: Control of Polymerization, Surface Coating, and Photopatterning. *Advanced Materials* 2014, 26:8029–8033.

[49] Lee M, Lee S-H, Oh I-K, Lee H: Microwave-Accelerated Rapid, Chemical Oxidant-Free, Material-Independent Surface Chemistry of Poly(dopamine). *Small* 2017, 13:1600443.

[50] Zhang C, Ou Y, Lei W-X, Wan L-S, Ji J, Xu Z-K: $CuSO_4/H_2O_2$-Induced Rapid Deposition of Polydopamine Coatings with High Uniformity and Enhanced Stability. *Angewandte Chemie International Edition* 2016, 55:3054–3057.

[51] Zeng Y, Du X, Hou W, Liu X, Zhu C, Gao B, et al.: Uv-Triggered Polydopamine Secondary Modification: Fast Deposition and Removal of Metal Nanoparticles. *Advanced Functional Materials* 2019, 29:1901875.

[52] Tan L, Tang W, Liu T, Ren X, Fu C, Liu B, et al.: Biocompatible Hollow Polydopamine Nanoparticles Loaded Ionic Liquid Enhanced Tumor Microwave Thermal Ablation *in vivo*. *ACS Applied Materials & Interfaces* 2016, 8:11237–11245.

[53] Xue J, Zheng W, Wang L, Jin Z: Scalable Fabrication of Polydopamine Nanotubes Based on Curcumin Crystals. *ACS Biomaterials Science & Engineering* 2016, 2:489–493.

[54] Chen F, Xing Y, Wang Z, Zheng X, Zhang J, Cai K: Nanoscale Polydopamine (PDA) Meets π-π Interactions: An Interface-Directed Coassembly Approach for Mesoporous Nanoparticles. *Langmuir* 2016, 32:12119–12128.

[55] Wu X, Zhou L, Su Y, Dong C-M: A Polypeptide Micelle Template Method to Prepare Polydopamine Composite Nanoparticles for Synergistic Photothermal-Chemotherapy. *Polymer Chemistry* 2016, 7:5552–5562.

[56] Ding T, Xing Y, Wang Z, Guan H, Wang L, Zhang J, et al.: Structural Complementarity from DNA for Directing Two-Dimensional Polydopamine Nanomaterials with Biomedical Applications. *Nanoscale Horizons* 2019, 4:652–657.

[57] Black KCL, Yi J, Rivera JG, Zelasko-Leon DC, Messersmith PB: Polydopamine-Enabled Surface Functionalization of Gold Nanorods for Cancer Cell-Targeted Imaging and Photothermal Therapy. *Nanomedicine* 2012, 8:17–28.

[58] Gong C, Lu C, Li B, Shan M, Wu G: Dopamine-Modified Poly(amino acid): An Efficient Near-Infrared Photothermal Therapeutic Agent for Cancer Therapy. *Journal of Materials Science* 2017, 52:955–967.

[59] Liu Y, Ai K, Liu J, Deng M, He Y, Lu L: Dopamine-Melanin Colloidal Nanospheres: An Efficient Near-Infrared Photothermal Therapeutic Agent for In vivo Cancer Therapy. *Advanced Materials* 2013, 25:1353–1359.

[60] Di Leo A, Curigliano G, Diéras V, Malorni L, Sotiriou C, Swanton C, et al.: New Approaches for Improving Outcomes in Breast Cancer in Europe. *The Breast* 2015, 24:321–330.

[61] Hamada A, Soh J, Mitsudomi T: Salvage Surgery After Definitive Chemoradiotherapy for Patients with Non-Small Cell Lung Cancer. *Translational Lung Cancer Research* 2021, 10:555–562.

©2022 The Authors. Creative Commons Attribution 4.0 International License

[62] Candido NM, de Melo MT, Franchi LP, Primo FL, Tedesco AC, Rahal P, et al.: Combining Photodynamic Therapy and Chemotherapy: Improving Breast Cancer Treatment with Nanotechnology. *Journal of Biomedical Nanotechnology* 2018, 14:994–1008.
[63] Wang K, Yu B, Pathak JL: An Update in Clinical Utilization of Photodynamic Therapy for Lung Cancer. *Journal of Cancer* 2021, 12:1154–1160.
[64] Qin S-Y, Zhang A-Q, Cheng S-X, Rong L, Zhang X-Z: Drug Self-Delivery Systems for Cancer Therapy. *Biomaterials* 2017, 112:234–247.
[65] Qin S-Y, Cheng Y-J, Lei Q, Zhang A-Q, Zhang X-Z: Combinational Strategy for High-Performance Cancer Chemotherapy. *Biomaterials* 2018, 171:178–197.
[66] Nam J, Son S, Ochyl LJ, Kuai R, Schwendeman A, Moon JJ: Chemo-Photothermal Therapy Combination Elicits Anti-Tumor Immunity Against Advanced Metastatic Cancer. *Nature Communications* 2018, 9:1074.
[67] Lo P-C, Rodríguez-Morgade MS, Pandey RK, Ng DKP, Torres T, Dumoulin F: The Unique Features and Promises of Phthalocyanines as Advanced Photosensitisers for Photodynamic Therapy of Cancer. *Chemical Society Reviews* 2020, 49:1041–1056.
[68] Wang W, Tang Z, Zhang Y, Wang Q, Liang Z, Zeng X: Mussel-Inspired Polydopamine: The Bridge for Targeting Drug Delivery System and Synergistic Cancer Treatment. *Macromolecular Bioscience* 2020, 20:2000222.
[69] Inguscio V, Panzarini E, Dini L: Autophagy Contributes to the Death/Survival Balance in Cancer Photodynamic Therapy. *Cells* 2012, 1:464–491.
[70] Castano AP, Demidova TN, Hamblin MR: Mechanisms in Photodynamic Therapy: Part One-Photosensitizers, Photochemistry and Cellular Localization. *Photodiagnosis and Photodynamic Therapy* 2004, 1:279–293.
[71] Song G, Ji C, Liang C, Song X, Yi X, Dong Z, et al.: Taox Decorated Perfluorocarbon Nanodroplets as Oxygen Reservoirs to Overcome Tumor Hypoxia and Enhance Cancer Radiotherapy. *Biomaterials* 2017, 112:257–263.
[72] Seth A, Lee H, Cho MY, Park C, Korm S, Lee JY, et al.: Combining Vasculature Disrupting Agent and Toll-Like Receptor 7/8 Agonist for Cancer Therapy. *Oncotarget* 2017, 8:5371–5381.
[73] Seth A, Gholami Derami H, Gupta P, Wang Z, Rathi P, Gupta R, et al.: Polydopamine-Mesoporous Silica Core–Shell Nanoparticles for Combined Photothermal Immunotherapy. *ACS Applied Materials & Interfaces* 2020, 12:42499–42510.
[74] Chen L, Zhou S-F, Su L, Song J: Gas-Mediated Cancer Bioimaging and Therapy. *ACS Nano* 2019, 13:10887–10917.
[75] Wang Y, Yang T, He Q: Strategies for Engineering Advanced Nanomedicines for Gas Therapy of Cancer. *National Science Review* 2020, 7:1485–1512.
[76] Wang Y-C, Dai H-L, Li Z-H, Meng Z-Y, Xiao Y, Zhao Z: Mesoporous Polydopamine-Coated Hydroxyapatite Nano-Composites for Ros-Triggered Nitric Oxide-Enhanced Photothermal Therapy of Osteosarcoma. *Journal of Materials Chemistry B* 2021, 9:7401–7408.
[77] Cheng W, Nie J, Xu L, Liang C, Peng Y, Liu G, et al.: pH-Sensitive Delivery Vehicle Based on Folic Acid-Conjugated Polydopamine-Modified Mesoporous Silica Nanoparticles for Targeted Cancer Therapy. *ACS Applied Materials & Interfaces* 2017, 9:18462–18473.
[78] Ding L, Zhu X, Wang Y, Shi B, Ling X, Chen H, et al.: Intracellular Fate of Nanoparticles with Polydopamine Surface Engineering and A Novel Strategy for Exocytosis-Inhibiting, Lysosome Impairment-Based Cancer Therapy. *Nano Letters* 2017, 17:6790–6801.
[79] Shi M, Zhang J, Li J, Fan Y, Wang J, Sun W, et al.: Polydopamine-Coated Magnetic Mesoporous Silica Nanoparticles for Multimodal Cancer Theranostics. *Journal of Materials Chemistry B* 2019, 7:368–372.
[80] Li Z, Yang F, Wu D, Liu Y, Gao Y, Lian H, et al.: Ce6-Conjugated and Polydopamine-Coated Gold Nanostars with Enhanced Photoacoustic Imaging and Photothermal/Photodynamic Therapy to Inhibit Lung Metastasis of Breast Cancer. *Nanoscale* 2020, 12:22173–22184.
[81] Lu Q, Lu T, Xu M, Yang L, Song Y, Li N: SO_2 Prodrug Doped Nanorattles with Extra-High Drug Payload for "Collusion Inside and Outside" Photothermal/pH Triggered - Gas Therapy. *Biomaterials* 2020, 257:120236.
[82] GhavamiNejad A, SamariKhalaj M, Aguilar LE, Park CH, Kim CS: pH/NIR Light-Controlled Multidrug Release via a Mussel-Inspired Nanocomposite Hydrogel for Chemo-Photothermal Cancer Therapy. *Scientific Reports* 2016, 6:33594.
[83] Zhang D, Wu M, Zeng Y, Wu L, Wang Q, Han X, et al.: Chlorin e6 Conjugated Poly(dopamine) Nanospheres as PDT/PTT Dual-Modal Therapeutic Agents for Enhanced Cancer Therapy. *ACS Applied Materials & Interfaces* 2015, 7:8176–8187.
[84] Li Y, Jiang C, Zhang D, Wang Y, Ren X, Ai K, et al.: Targeted Polydopamine Nanoparticles Enable Photoacoustic Imaging Guided Chemo-Photothermal Synergistic Therapy of Tumor. *Acta Biomaterialia* 2017, 47:124–134.
[85] Chen Y, Ai K, Liu J, Ren X, Jiang C, Lu L: Polydopamine-Based Coordination Nanocomplex for T1/T2 Dual Mode Magnetic Resonance Imaging-Guided Chemo-Photothermal Synergistic Therapy. *Biomaterials* 2016, 77:198–206.
[86] Liu B, Li C, Xing B, Yang P, Lin J: Multifunctional UCNPs@PDA-ICG Nanocomposites for Upconversion Imaging and Combined Photothermal/Photodynamic Therapy with Enhanced Antitumor Efficacy. *Journal of Materials Chemistry B* 2016, 4:4884–4894.
[87] Yan S, Zeng X, Tang Y, Liu B-F, Wang Y, Liu X: Activating Antitumor Immunity and Antimetastatic Effect through Polydopamine-Encapsulated Core–Shell Upconversion Nanoparticles. *Advanced Materials* 2019, 31:1905825.
[88] Wu L, Zhang F, Wei Z, Li X, Zhao H, Lv H, et al.: Magnetic Delivery of Fe_3O_4@polydopamine Nanoparticle-Loaded Natural Killer Cells Suggest a Promising Anticancer Treatment. *Biomaterials Science* 2018, 6:2714–2725.
[89] Zhuang H, Su H, Bi X, Bai Y, Chen L, Ge D, et al.: Polydopamine Nanocapsule: A Theranostic Agent for Photoacoustic Imaging and Chemo-Photothermal Synergistic Therapy. *ACS Biomaterials Science & Engineering* 2017, 3:1799–1808.
[90] Wang H, Wang W, Liu L, Wang M, Li G, Li H, et al.: Biodegradable Hollow Polydopamine@manganese Dioxide as an Oxygen Self-Supplied Nanoplatform for Boosting Chemo-Photodynamic Cancer Therapy. *ACS Applied Materials & Interfaces* 2021, 13:57009–57022.
[91] Zhang T, Jiang Z, Xve T, Sun S, Li J, Ren W, et al.: One-Pot Synthesis of Hollow PDA@DOX Nanoparticles for Ultrasound Imaging and Chemo-Thermal Therapy in Breast Cancer. *Nanoscale* 2019, 11:21759–21766.
[92] Li M, Sun X, Zhang N, Wang W, Yang Y, Jia H, et al.: NIR-Activated Polydopamine-Coated Carrier-Free "Nanobomb" for In Situ On-Demand Drug Release. *Advanced Science* 2018, 5:1800155.

©2022 The Authors. Creative Commons Attribution 4.0 International License